

1 Postprint of: Kolerski T., Assessment of the ice jam potential on regulated rivers and reservoirs with the use of
2 numerical model results, COLD REGIONS SCIENCE AND TECHNOLOGY, Vol. 191, iss. 11 (2021), 103372,
3 DOI: [10.1016/j.coldregions.2021.103372](https://doi.org/10.1016/j.coldregions.2021.103372)

4

5 © 2021. This manuscript version is made available under the CC-BY-NC-ND 4.0
6 license <https://creativecommons.org/licenses/by-nc-nd/4.0/>

7

8 Assessment of the ice jam potential on regulated rivers and reservoirs with 9 the use of numerical model results

10 Tomasz Kolerski

11 Gdańsk University of Technology, Faculty of Civil and Environmental Engineering,
12 Narutowicza 11/12, 80-233 Gdańsk, Poland
13 tomasz.kolerski@pg.edu.pl

14 **Abstract**

15 This study presents an attempt at estimating the jam potential on rivers with significant
16 anthropogenic intervention in the course or flow characteristics of the river. The DynaRiCE model
17 was used for forecasting both the place and time of an ice jam occurrence. In this modified method,
18 two ice parameters are subjected to analysis, namely the relative ice-to-water velocity (v_i/v_w), and
19 the ice thickness to single floe thickness (η_i/η_0). Both variables were analyzed at two locations; first
20 spot is the Odra River near Słubice-Frankfurt bridge (between 581 and 586 km), and the second is the
21 Vistula section between the existing Włocławek dam (674.75 river km) and the planned Siarzewo
22 dam (706.38 river km), covering a 31.6 km reach. Once the model is implemented in the selected
23 areas, the numerical simulations were processed and the obtained results were analyzed in terms of
24 ice accumulation and jamming. The results on both rivers shown some potential of ice jamming, due
25 to the planned engineering works. In the case of the Odra river, it was indicated that ice jam
26 potential increased during the ice run of high concentration in the average flow conditions. For the
27 Vistula river two locations for ice jamming were designated and for both of the points an increase of
28 the ice thickness by about 60 % from the initial, single flow thickness was observed. Also in this case,
29 the area-averaged ice velocity in an initially specified location drops below 15% of the average water

30 velocity in that area. According to the used methodology, both cases are classified as 'ice jam
31 probable' type.

32 **Keywords:** ice dynamics; ice jams; river engineering; Odra River; Vistula River

33 **1 Introduction**

34 A common issue in engineering practice is to estimate the ice congestion and jamming potential of
35 rivers due to planned river engineering works or new run-of-river reservoirs and diversion dams. The
36 task most often comes down to determining to what extent hydrotechnical structures will affect ice
37 transport, and whether or not they will not stop the ice run during freeze-up and during spring or
38 mid-winter breakup. In order to consider the fragmented ice cover at locations where border ice has
39 grown across the river or where man-made structures form a surface barrier, drifting ice can
40 accumulate and progress upstream (Svensson et al., 1989). This issue is not a trivial task and above
41 all requires the determination of the impact of hydro-engineering structures on the ice dynamics.
42 Analyses should additionally take into account other factors affecting ice flow; i.e., wind speed and
43 direction, hydrological and meteorological factors, as well as flow regulation through diversion
44 structures (Ashton, 1978; Grześ, 1991; Lal and Shen, 1991; White, 1999).

45 Historical observations provide a vision for researchers to know the severity of the ice-related flood
46 damaging. Floods are most likely to occur on rivers that have experienced flooding in the past.
47 Despite this, potential flood hazard may be unknown to some residents and local authorities, due to
48 the long intervals of flood or the resident's recent arrival in the area (Kovachis et al., 2017). It is
49 needed to be considered that reoccurring the ice jams may cause the geometric impacts on the river
50 basins (Boucher et al., 2009). From an ecosystem perspective, a longer-term view may be more
51 important than annual predictability (Timoney et al., 1997). Having access to data set, it is possible to
52 illustrate how ice regime characteristics may have varied through time and space within the cold-
53 region watercourse and examine some of the potential geomorphic responses associated with ice
54 jam dynamics (Boucher et al., 2012). An important consideration is the inherent uncertainty in these

55 data sets, which must be factored into assessment of ice-jam flood history (Wolfe et al., 2020).
56 Although, statistical information of ice processes helps to understand general trends in ice cover
57 formation and ice movement, the complexity of the processes makes it nearly impossible to achieve
58 a higher accuracy level (Kolerski, 2018). To predict water levels that can potentially occur as a result
59 of ice jamming, it is necessary to apply one of several numerical models that are available. Regardless
60 of which model is selected for application, certain hydraulic and morphologic data sets are needed
61 (Beltaos and Burrell, 2015). However, by utilizing existing theories, a mathematical model of these
62 processes can be developed. Such model can be used to provide a continuous description of river ice
63 development based on a limited amount of field data. The model can also assist engineers in
64 evaluating the possible beneficial and detrimental consequences of ice-control structures and flow
65 regulation (Lal and Shen, 1991).

66 Following the model selection, the results of the modeling run, as well as scenarios of ice jams of
67 different length and locations can be concluded (Beltaos, 2018). To quantify which factor influences
68 the formation of ice jamming the most, a local parameter sensitivity analysis can be carried out to
69 calculate the sensitivity of different parameters on ice jam flooding (Das and Lindenschmidt, 2020).
70 In other words, a sensitivity analysis can be performed to evaluate changes in model predictions
71 resulting from changes in several model input parameters. The parameters like: river flow rate,
72 locations of ice jam formation, ice supply volume entering from upstream, downstream water level,
73 and underside roughness (i.e. Manning's coefficient) of the ice cover and jam (Liu and Shen, 2005).

74 In recent years, knowledge about ice processes on rivers has been significantly improved, which is
75 reflected in the developed mathematical models for simulating flow in rivers in winter conditions.
76 The initial concept of the static ice jam theory, first developed by (Pariset et al., 1966; Pariset and
77 Hauser, 1961) is based on a static balance of floating ice. It was further developed by (Uzuner and
78 Kennedy, 1976, 1974) and used in a number of mathematical models. The basic ice jam stability
79 concepts are categorized under common modular feature, and have been adopted in a number of

80 one-dimensional mathematical models, including the RIVJAM model developed by (Beltaos, 1983;
81 Uzunur and Kennedy, 1976, 1974), the ICEJAM model (Flato and Gerard, 1986), RIVER1D (Hicks et al.,
82 1992) and RIVICE (Lindenschmidt et al., 2012). Moreover, the theory behind the ice module in
83 commercial softwares, such as the HEC RAS model or the MIKE11-ICE model closely follow static jam
84 formulations (Brunner, 2002; Thériault et al., 2010). Since an ice jam is fully dynamic and three-
85 dimensional in nature, modeling its occurrence and range often requires a more sophisticated
86 approach. Therefore, Shen developed DynaRICE, a two-dimensional, depth-averaged coupled
87 hydrodynamic and ice dynamic model of ice transport in rivers (Shen, 2010; Shen et al., 2000).

88 In the context of what can be defined in a broad sense as the impact assessment of river ice
89 phenomena, one-dimensional modeling has been widely used to recreate magnitude of ice related
90 flooding and maximum water levels reached in the river valley (Beltaos, 2003; Kandamby et al., 2010;
91 Lindenschmidt et al., 2019; Lindenschmidt and Rokaya, 2019). In such an approach, model efficiency
92 is significantly improved, however it assumes a regular distribution of ice velocity and thickness in a
93 cross section. Therefore a two-dimensional model is implemented in the area, where a blockage is
94 expected to occur (Shen and Liu, 2003; Su et al., 1997; Kolerski and Shen, 2015).

95 **1.1 Study site**

96 When selecting the model domain, it is important to refer to historical data and other evidence,
97 including practical knowledge from the management of water systems and icebreaker crews. On this
98 basis, river sections with a significant ice jam potential were determined, which were subjected to
99 detailed numerical analyses. The assessment of the results of the numerical model in the context of
100 the risk of an ice jam requires the area to be determined in which ice run slows noticeably and
101 increases in concentration and thickness. Such locations are often places where the water flow
102 diverges due to the existence of an island (Pawłowski, 2015), rapids or in the case of the channel
103 being split into a number of distributaries (i.e. the ice jam in the St Clair delta (Kolerski and Shen,
104 2015)). Furthermore, a reduction in the slope of the river bed or the water level (ice inflow to a

105 reservoir (Rădoane et al., 2010)), a narrowness in the channel as well as the presence of engineering
106 structures, such as bridge piers will hamper ice transport (Wang et al., 2015).

107 1.1.1 Odra River

108 A good example in ice accumulation area, is a section of the natural border river - the Odra, which is
109 characterized in terms of ice jamming potential by the Regional Water Management Board in
110 Szczecin (RWMB Szczecin). Information on jam-prone sections of the Odra River mainly comes from
111 observations made during annual icebreaking operations and published reports (RWMA, 2010).



112

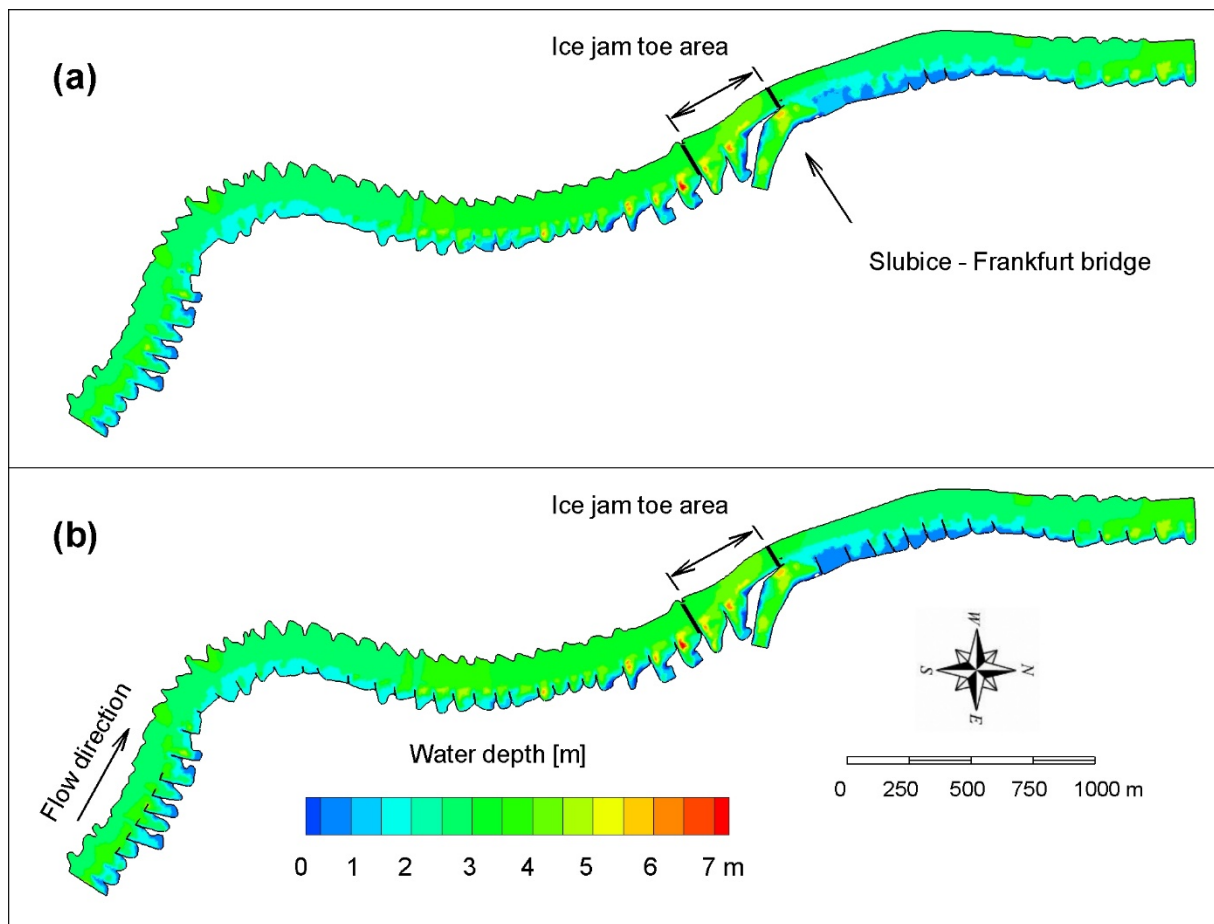
113 **Figure 1. The catchment of the Upper and Middle sections of the Odra River**

114 The Odra River, similar to many European rivers, was modified in the mid-18th century to establish
115 stable conditions for navigation, and reduce bank erosion. Early river engineering works on the Odra
116 River were mainly carried out by the construction of closure structures, built across secondary

117 channels to reduce floodplain conveyance and increase the main channel depth. The process was
118 carried out until the middle of the 20th century and caused a significant reduction in large winter
119 flooding (Mudelsee et al., 2004). However, it did not affect the ice jam potential of the river.
120 Currently, according to the Regional Water Management Authority in Szczecin (RWMA Szczecin), the
121 lower section of the Odra River (about 200 km), which is a natural border between Poland and
122 Germany, has 28 ice jam prone locations extending over more than one fourth of the river.

123 The Polish city of Słubice is located on the banks of the Odra River, which forms the border with
124 Germany. According to RWMA Szczecin, the river in the vicinity of the city is particularly susceptible
125 to ice jamming. As shown in (Kolerski, 2018), this is caused by the river narrowness and an additional
126 reduction in the cross-section triggered by a single bridge pier (Słubice-Frankfurt bridge). In recent
127 years, the city was at risk of flooding caused by ice jamming, e.g. in February 2010. Within the Odra-
128 Vistula Flood Management Project (OVFMP), it is planned to rehabilitate all the existing structures on
129 a 5 km reach of the river. The proposed system of spurs is designed in the form of extensions of the
130 existing structures which are damaged to a varying degree (Kreft and Parzonka, 2007).

131 Detailed river bathymetry and shoreline data measured in 2017 for the OVFMP, are used for the
132 study. The data is considered to represent the current state of the river, which is considered to be
133 substantially rebuilt by the construction or reconstruction of spur dikes within the OVFMP. The
134 conditions after project implementation are taken into account in the model domain by changing the
135 shoreline to include all the proposed structures. Within the model domain, a sub-domain was
136 selected where a quantitative jam analysis was conducted. The area includes a river section of about
137 450 m long upstream of the Słubice – Frankfurt bridge. The location was selected based on the
138 general trend in ice transport and the high potential of that area for ice jamming and accumulation.
139 Quantitative comparisons of both the current and proposed river conditions for all the simulated
140 cases are presented in Figure 2. The modifications are on the left bank along the whole river section,
141 where the spur dikes are proposed.



142

143 **Figure 2** Water depth at average flow ($Q_w = 276 \text{ m}^3/\text{s}$) for current (a) and proposed (b) conditions; sub-domain for
 144 numerical jam analysis designated by arrow

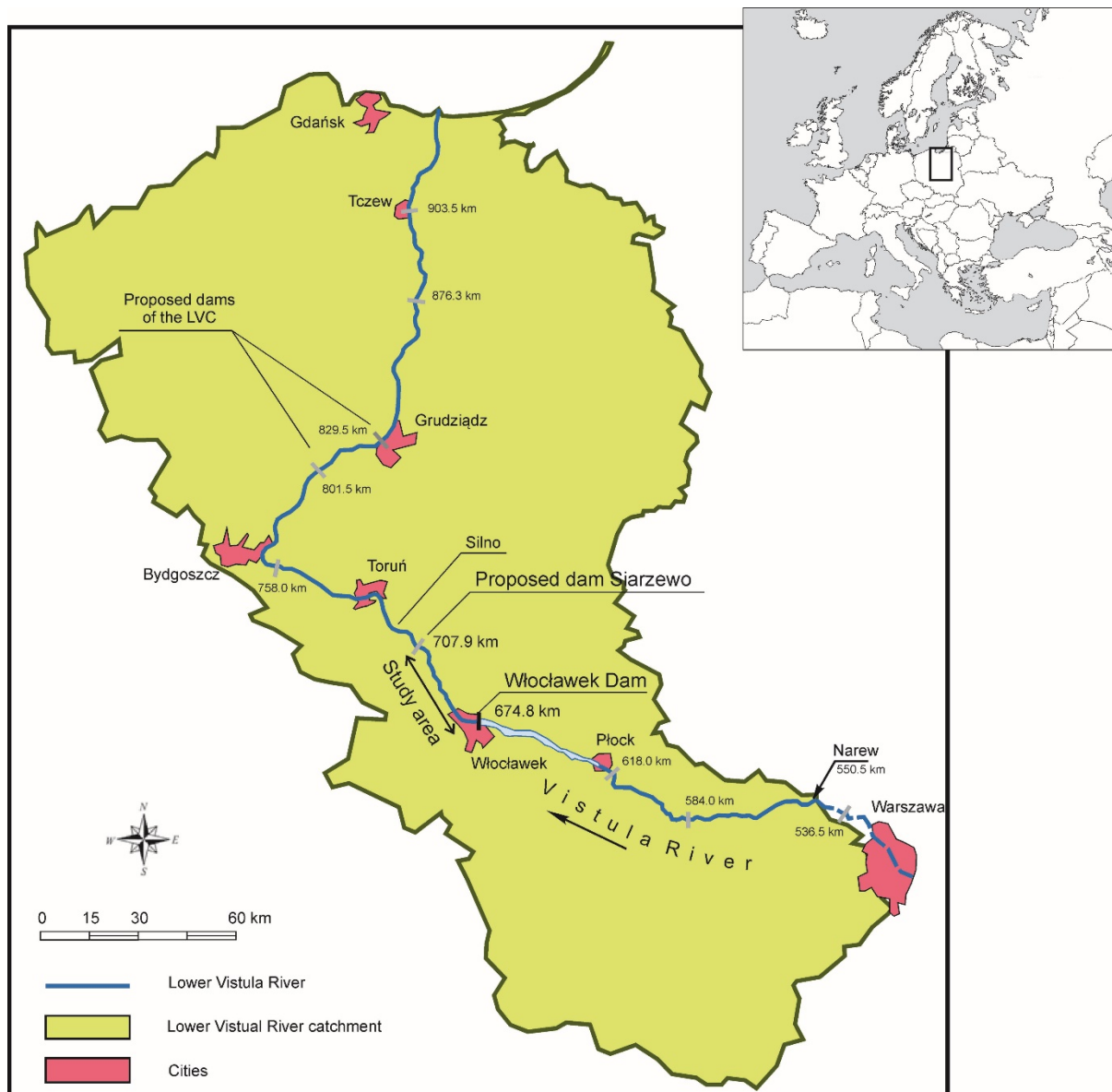
145 1.1.2 Vistula River

146 If the area of interest has no historical evidence of ice jamming or its hydrodynamic features can
 147 change significantly based on an executed river regulation plan, the entire reach should be included
 148 in the mathematical modeling to the extent possible. Such is the case with regard to the Vistula
 149 River, where a new reservoir is planned to be accomplished by the construction of a new dam in
 150 Siarzewo, located at 706.4 river kilometers, which is about 30 km downstream of the existing
 151 Włocławek dam.

152 Unlike the Odra, the Vistula River was regulated fragmentarily at the second half of the 19th century.
 153 The river was divided between three countries, and only in the lower section (downstream of Silno –
 154 see Figure 3), which formerly belonged to Prussia,)river engineering works proceeded to a large
 155 extent. Currently, the river is in a state of gradual deterioration due to a lack of attention to

156 engineering works (Szymkiewicz, 2017). In addition, Włocławek diversion dam (the only reservoir
157 functioning on the Vistula River) contributed to river degradation due to a pulsed water discharge
158 which intensified the erosion downstream of the channel. From the beginning of the operation in the
159 1970s until the 1990s, the hydropower plant provided peak power demand, temporarily causing
160 rapid flow changes. The water discharge in the Vistula varied from about 400 m³/s during off-peak
161 periods to as high as 2000 m³/s during peak operation (Babiński, 1982; Gosztowtt, 2018).

162 Włocławek diversion dam is a part of a low-head dam cascade developed in the 1950s (Szydłowski et
163 al., 2015). The main purpose of the concept was to improve the Polish hydropower development
164 potential and protection against flooding and water resource management for agricultural fields
165 threatened by the draught. Recently, due to economic development and resultant increased traffic
166 requirements from the Baltic Sea port (Gdańsk) to the south of the country, and removing electricity
167 inadequacy in northern Poland have stimulated welcoming the old concept of the Lower Vistula
168 Cascade operation (LVC). Siarzewo dam was first proposed at 706.38 river km, and the project is
169 currently being designed (Kolerski, 2016).



170

171 **Figure 3** The Lower sections of the Vistula River—the black bars indicate locations for the proposed dams within the LVC,
 172 with river mileage

173 **1.2 Ice condition description**

174 **1.2.1 Odra river**

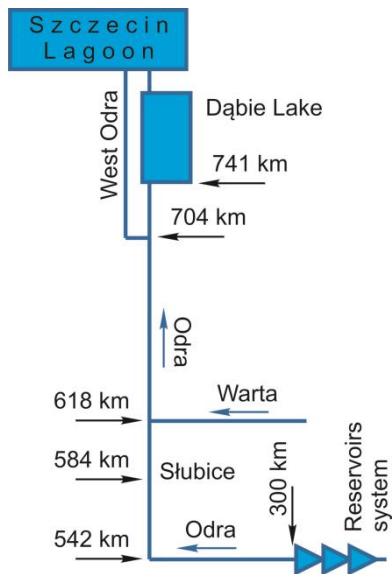
175 The ice cover on the Odra River is dominantly formed from dynamic ice accumulation. A sketch of the
 176 lower and middle Odra River is shown in Figure 4. Typically, the process of ice cover development is
 177 initiated at Dąbie Lake, where static ice cover is formed first. Next, incoming ice floes may stop at the
 178 leading edge of the ice cover on the lake or flow underneath the cover (Kolarski, 2018; Marszelewski
 179 and Pawłowski, 2019). The rate of ice cover progression in the upstream direction is affected by the
 180 water flow and ice conditions, as well as the high water levels on the Southern Baltic Sea through the

181 backwater effect and meteorological conditions. Ice cover formed from the accumulation of dynamic
182 floes has a big potential for jam formation, as evidenced by yearly ice reports provided by RWMA
183 Szczecin.

184 Besides natural processes, another important mechanism affecting the ice run is ice sluicing from the
185 system of low-head reservoirs in the middle section of the Odra River (see Figure 4). It is noteworthy
186 that a lack of coordinated icebreaking operations on the Odra and on the mentioned reservoirs could
187 significantly increase the threat of ice jamming on the downstream section of the river. Such a
188 situation occurred in February 2010, when ice sluicing started without prior consultation with the
189 management of the Polish-German icebreaking operation. Breaking the ice on reservoirs and sluicing
190 it through the spillways require an increment in discharge, which forms a surge in the downstream
191 river section. To avoid uncontrolled breakup at the downstream section of the river, the surges must
192 be evenly distributed over time. If ice sluicing occurs long before the icebreakers reach the edge of
193 ice cover which is located at the upstream end of the reservoir along the river channel, the broken
194 ice from the sluicing operation accumulates at the intact ice cover downstream of the spillway.

195 In the winter season of 2009-2010, 250 km of the Odra was covered by ice, and the leading edge of
196 the ice cover reached the station of 491.4 km of the river. In the second part of February due to air
197 temperatures above zero, the strength of the ice cover reduced; however, it still remained intact in a
198 large portion of the river (645 - 491 river km). Regardless of the situation in the lower section of the
199 river, an ice-sluicing operation from the reservoirs was started. Realizing the threat, icebreaker crews
200 worked on the Odra with a great nonstop effort. On 27th February, the bridge in Słubice was reached
201 by the icebreakers and an ice-free channel was formed. During the night of 28th February, the
202 weakened ice cover started to collapse due to the additional ice mass released from the reservoirs,
203 and a large amount of ice collapsed forming an uncontrolled breakup. Under these life-threatening
204 conditions, the icebreakers were forced to flee downstream, hiding in the Warta outlet (see photo
205 taken on 28th February, 2010, shown in Figure 5).





206

207 Figure 4 Schematic view of the Middle and Lower Odra River (Note: figure out of scale)



208

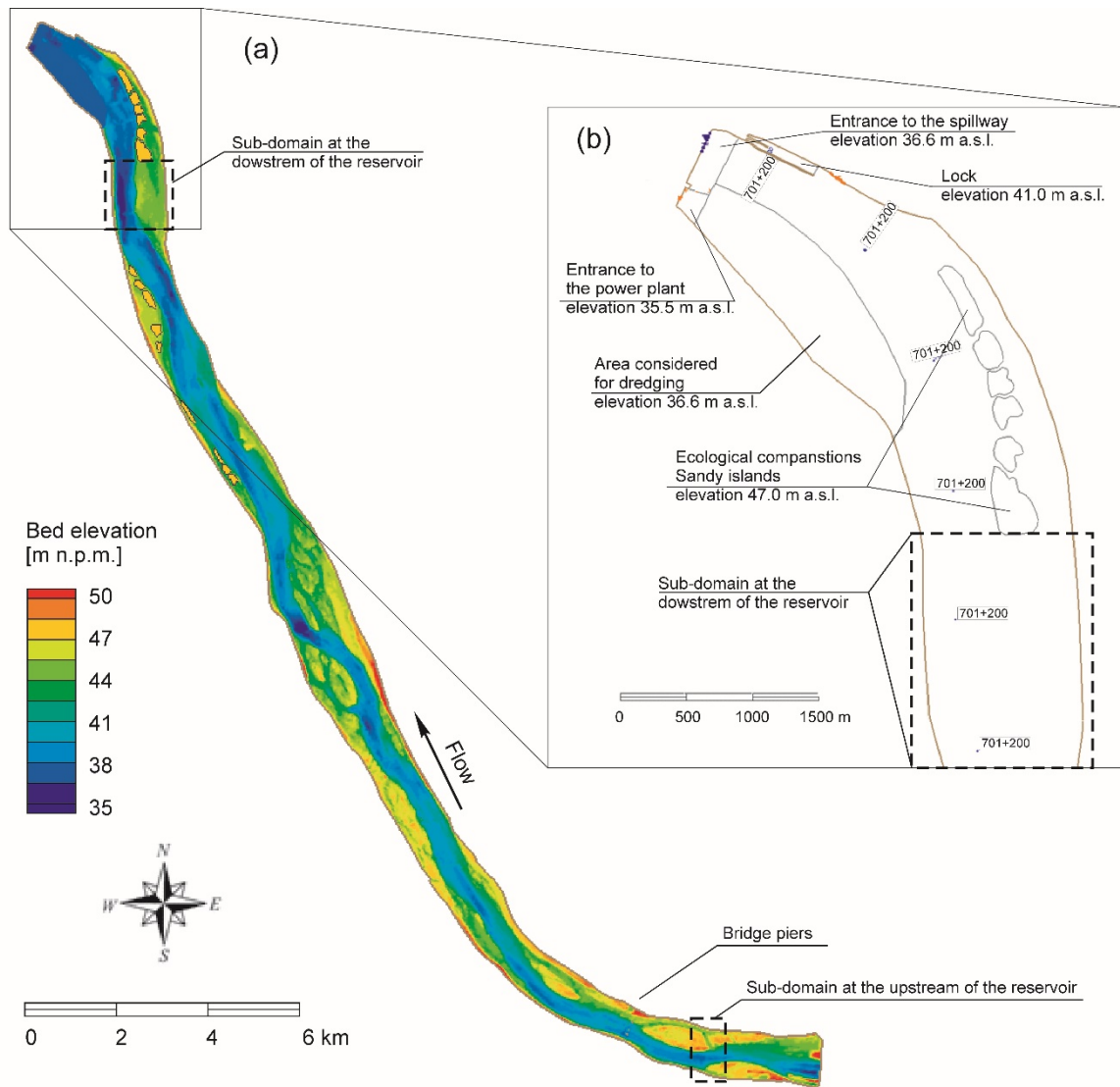
209 Figure 5 Polish and German icebreakers escaping to the Warta River on 28th February, 2010 (railroad bridge at 615.1
210 river km) (RWMA, 2010)

211 1.2.2 Vistula river

212 The study covered the Vistula section between the existing Włocławek dam (674.75 river km) and the
213 planned Siarzewo dam (706.38 river km), covering a 31.6 km reach. In this section, ice processes are
214 affected by existence of the first locating dam and will be significantly changed due to new Siarzewo
215 project. The bathymetry of the model domain was described by 32 cross-sections surveyed by the
216 Institute of Meteorology and Water Resources in April 2018, reported by the National Water
217 Management Authority 'Wody Polskie' (NWMA). Topographic data were developed on the basis of a
218 digital elevation model obtained from the state of geodetic resources
219 <https://pzgik.geoportal.gov.pl/imap>; with a resolution of 1cm in vertical and horizontal direction.

220 In addition, the model domain includes the proposed elevation of the entrance area of the spillway
221 (36.6 m above sea level) and the proposed entrance basin of the hydropower plant (35.5 m above
222 sea level). Also, the left floodplain of the river bank located immediately upstream of the planned
223 hydroelectric power plant requires dredging. It was assumed that the area would be dredged to a
224 level of 36.6 m a.s.l. Bathymetric data together with topographic data used to build the mathematical
225 model are shown in the Figure 6.

226 The existence of artificial islands has been taken into account in all simulations. A total number of 15
227 islands are designed, as part of an ecological compensation scheme, along both banks of the reservoir.
228 The islands were proposed to provide habitat areas for birds (i.e. common tern, little ringed plover,
229 kingfisher) nesting in the river shoals which will be flooded due to the creation of the reservoir. Thus,
230 the islands are designed in the form of sandy areas exposed over the normal water level, and mildly
231 sloping beaches. It was assumed that the shoreline of each island is at the normal pool level of the
232 proposed reservoir (46.0 m a.s.l), and the central part of each island is flat and exposed by 1 m above
233 the pool level (47.0 m a.s.l.). The shorelines, are shown in Figure 6b, while the bathymetry of the area,
234 including the islands, is shown in Figure 6a.

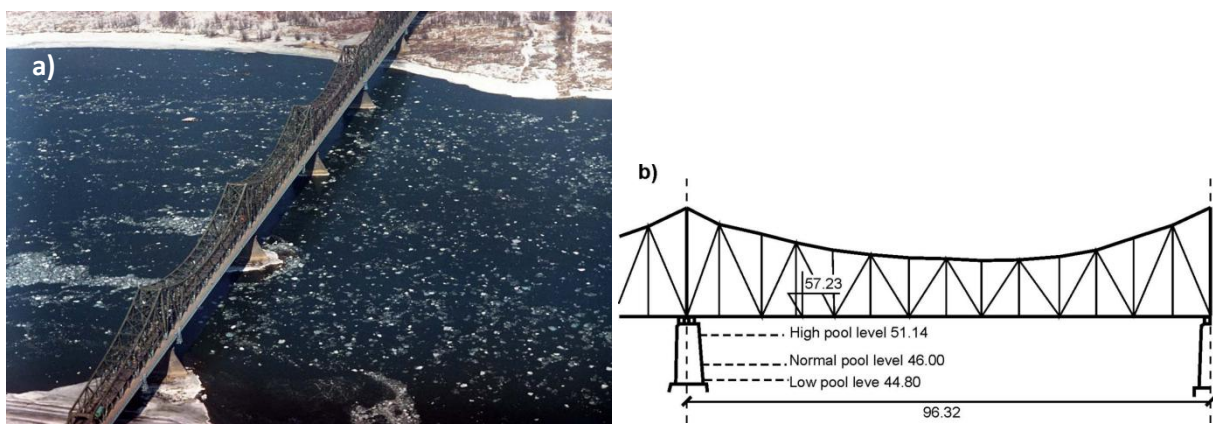


235

236 **Figure 6 Siarzewo reservoir bathymetry included in the mathematical model showing islands and sub domain areas (a);**
 237 **downstream section of the model domain all the areas of modified bathymetry (b)**

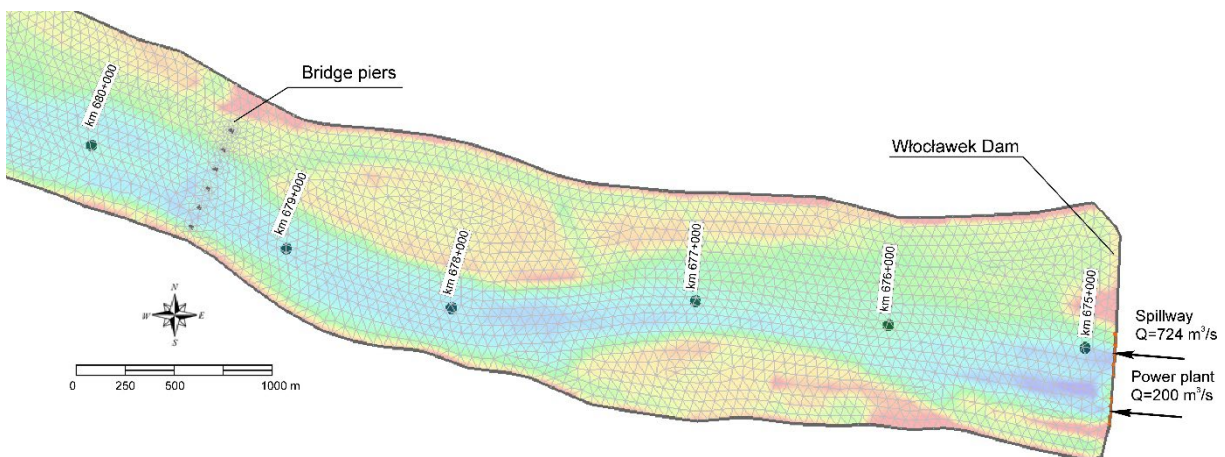
238 In the downstream section of the reservoir, the area adjacent to the Vistula left bank is a low-lying
 239 floodplain with riparian vegetation and wetlands which support a rich ecosystem. Due to the dam
 240 construction, the pool level in the reservoir will cause a floodplain area, which will be permanently
 241 inundated. Thus it is necessary to ensure that potentially deteriorated habitats are recreated by the
 242 planning of sandy islands to be built in the reservoir. The group of 6 islands is proposed close to the
 243 dam (about 3.5 km upstream) and, as shown by the numerical results, these islands significantly
 244 threaten the ice run.

245 In the upper section of the reservoir, about 4.5 km downstream from Włocławek dam, there is a bridge
 246 which deck is supported by 6 piers with semi-circular ends, 96.32 m apart from each other (Figure 7).
 247 All piers will be in the wetted area, once the pool level is achieved in the new reservoir. The bridge
 248 piers located within the route of the ice run will hamper its movement downstream, and could cause
 249 ice jamming (Szydlowski and Kolerski, 2018). Due to the significant impact of these bridge piers on the
 250 ice dynamics in the immediate vicinity of Włocławek dam, they were included in the model in the form
 251 of a closed land boundary, as shown in Figure 8.



252

253 **Figure 7** Frazil and pancake ice runs under the bridge in Włocławek, photo courtesy of prof. Marek Grześ (a); a typical
 254 section of the bridge at 679+200 river km (b)



255

256 **Figure 8** Upstream section of the model domain showing finite element mesh with bridge pier locations, river mileage
 257 and upstream boundary conditions for average flow $Q_{ave} = 924 \text{ m}^3/\text{s}$

258 1.3 Model description

259 The DynaRICE model allows the forecasting of both the place and time of an ice jam occurrence (Knack
 260 and Shen, 2018; Kolerski and Shen, 2015). The DynaRICE model is able to provide information on the

261 spatial and temporal distribution of ice in a river with a minimal user intervention limited to the task
 262 of the inputting data such as bathymetry, meteorological conditions and hydrodynamic data on the
 263 open boundaries of the domain (Carson et al., 2011). This means that the user does not need to know
 264 a priori location of the ice jam toe or the time of its formation. This is particularly important in the case
 265 of simulating processes resulting from planned structures (Knack and Shen, 2017). Then, objectively,
 266 only on the basis of the balance of forces and other external factors, can information on potential ice
 267 accumulation and jamming be obtained. In order to reduce computation effort, the modelling domain
 268 is limited to only areas where ice jams are expected to occur. The domain includes locations important
 269 from ice jamming processes point of view without expansion of the calculation time to a great extent.
 270 The model was set up to simulate the ice run in the typical flow expected at the beginning of the winter
 271 season and breakup conditions. The hydrodynamic module is based on the mass and momentum
 272 equations including mutual interaction between ice and water flow that are shown in conservation
 273 form (Shen et al., 1990):

$$\frac{\partial H_w}{\partial t} + \frac{\partial q_x}{\partial x} + \frac{\partial q_y}{\partial y} = \frac{\partial}{\partial t} (N\eta'), \quad (1-1)$$

$$\frac{\partial q_x}{\partial t} + \frac{\partial}{\partial x} \left(\frac{q_x^2}{H_w} \right) + \frac{\partial}{\partial y} \left(\frac{q_x q_y}{H_w} \right) = \frac{1}{\rho} (\tau_{sx} - \tau_{dx}) + \frac{1}{\rho_w} \left(\frac{\partial T_{xx}}{\partial x} + \frac{\partial T_{yx}}{\partial x} \right) - g H_w \frac{\partial h}{\partial x}, \quad (1-2)$$

$$\frac{\partial q_y}{\partial t} + \frac{\partial}{\partial x} \left(\frac{q_x q_y}{H_w} \right) + \frac{\partial}{\partial y} \left(\frac{q_y^2}{H_w} \right) = \frac{1}{\rho} (\tau_{sy} - \tau_{dy}) + \frac{1}{\rho_w} \left(\frac{\partial T_{xy}}{\partial x} + \frac{\partial T_{yy}}{\partial x} \right) - g H_w \frac{\partial h}{\partial y}. \quad (1-3)$$

274 In which q_x and q_y denote water discharge in x and y directions (the flow under the ice cover and
 275 seepage flow through the ice); h is water surface elevation [m]; η' indicates ice thickness from the
 276 underside surface to the water level [m]; τ_{sx} and τ_{sy} are shear stresses on the water surface in x and y
 277 direction [Pa]. It either refers to the shear stress on the underside surface of the ice ($\tau_{ix,y}$) or the
 278 water surface caused by the wind ($\tau_{ax,y}$); τ_{dx} and τ_{dy} are shear stress on the river bed in x and y
 279 direction [Pa]; N is ice concentration [-]; ρ_w is water density [$\text{kg}\cdot\text{m}^3$]; H_w denotes total water depth
 280 underneath an equivalent ice-water interface $H_w/d_w = q/q_s$ [m]; d_w is water depth under the ice;

281 q_s is seepage discharge. T_{xy} is a turbulence tensor. Bed shear stress is calculated from (Shen et al.,
282 1990):

$$\tau_{dx} = \frac{n_d^2}{(\alpha_d d_w)^{1/2}} \rho g \frac{q_x (q_x^2 + q_y^2)^{1/2}}{d_w^2}, \quad (1-4)$$

$$\tau_{dy} = \frac{n_d^2}{(\alpha_d d_w)^{1/2}} \rho g \frac{q_y (q_x^2 + q_y^2)^{1/2}}{d_w^2}. \quad (1-5)$$

283 Parameter α_d is the fraction of the water depth affected by the bed friction, $\alpha_d = A_d/A$; n_d is the
284 Manning's roughness coefficient for river bed. On open water surface, the wind shear stress on water
285 surface is calculated from (Shen, 2016):

$$\tau_{a,x} = C_w \rho_a V_a^2 \cos \xi_a, \quad (1-6)$$

$$\tau_{a,y} = C_w \rho_a V_a^2 \sin \xi_a. \quad (1-7)$$

286 In which ξ_a is the angle of wind vector (between wind direction and x axis); $C_w = 0.00155$, is wind
287 drag coefficient (Wu, 1973); V_a is wind velocity; ρ_a is air density.

288 In the DynaRICE model the dynamic transport of the river ice is mathematically described as the
289 movement of the number of particles carrying all ice properties and being subjected to the force
290 balance. The governing equation for ice dynamics can be presented in the following form (Shen et al.
291 2000):

$$M_L \frac{d\vec{V}_L}{dt} = \vec{R} + \vec{F}_a + \vec{F}_w + \vec{G} \quad (1-8)$$

292 In which M_L is mass per area of parcel, \vec{V}_L is ice velocity vector, $\frac{d\vec{V}_L}{dt}$ is surface ice acceleration, \vec{R} is an
293 ice internal resistance force, \vec{F}_a is a wind drag force, \vec{F}_w is a water drag force, \vec{G} is gravitational force.
294 In two dimensional coordinate system (depth averaged), internal ice resistance can be described in
295 following way (Shen et al., 2000):

$$\vec{R} = iR_x + jR_y, \quad (1-9)$$

$$R_x = \frac{\partial}{\partial x} (\sigma_{xx} N \eta) + \frac{\partial}{\partial y} (\sigma_{xy} N \eta), \quad (1-10)$$

$$R_y = \frac{\partial}{\partial x} (\sigma_{yx} N \eta) + \frac{\partial}{\partial y} (\sigma_{yy} N \eta), \quad (1-11)$$

296 In which, σ_{xx} and σ_{yy} are internal ice stresses in normal direction built up in ice rubble, $\sigma_{xy} = \sigma_{yx}$ are
 297 internal ice stresses in tangential direction. Internal stresses are calculated from viscoelastic–plastic
 298 constitutive model with Mohr-Coulomb yielding criterion for the ice as described in (Ji et al., 2005).
 299 Other terms from equation (1-8); .i.e. wind and water drag, as well as gravitational force can be
 300 calculated as follows:

$$\vec{F}_a = \vec{i} \left[\rho_a C_w \left| \vec{V}_L - \vec{W} \right| (u - W_x) N \right] + \vec{j} \left[\rho_a C_w \left| \vec{V}_L - \vec{W} \right| (v - W_y) N \right] \quad (1-12)$$

$$\vec{F}_w = \vec{i} \left[\rho \frac{n_L^2}{(\alpha_d d_w)^{1/2}} \left| \vec{V}_L - \vec{V}_w \right| (u - u_w) N \right] \quad (1-13)$$

$$+ \vec{j} \left[\frac{n_L^2}{(\alpha_d d_w)^{1/2}} \left| \vec{V}_L - \vec{V}_w \right| (v - v_w) N \right]$$

$$\vec{G} = -\vec{i} M_L g \left(\frac{\partial \eta}{\partial x} \right) - \vec{j} M_L g \left(\frac{\partial \eta}{\partial y} \right) \quad (1-14)$$

301 $\vec{V}_w = u_w \vec{i} + v_w \vec{j}$ is water velocity vector, $\vec{V}_L = u \vec{i} + v \vec{j}$ is surface ice velocity vector, $\vec{W} = \vec{W}_x \vec{i} +$
 302 $\vec{W}_y \vec{j}$ is a wind velocity vector referred to the wind velocity on 10 m height above the water surface,
 303 n_L is ice roughness, d_w is a water depth under the ice[m]. The solution of the unsteady
 304 hydrodynamics is based on the Finite Element method (explicit upwind Galerkin scheme), and for the
 305 ice dynamics, the Smoothed Particle Hydrodynamic (SPH) method is used (Shen et al., 2000).

306 1.3.1 Model parameters description

307 The DynaRICE model has many parameters that must be determined or calibrated by the user. The
 308 most influential physical and numerical parameters are presented in Table 1. Considering the single
 309 layer ice and ice accumulation, the default values for the Manning's coefficients were used; however,
 310 to include local characteristics of the ice, the values varied for both sites. At Vistula River, the ice will
 311 be delivered from the reservoir located at the upstream open boundary. Thus, the ice entering the
 312 domain is the fragmented static ice cover from the reservoir, which its underside is smooth ($n_i =$
 313 $0.02 \text{ s} \cdot \text{m}^{-1/3}$ was used). At the Odra River, the ice is mainly from the fragmented static ice cover,

314 originated from the system of reservoirs located at a longer distance (approximately 100 km) in
 315 comparison with Vistula River. Since the distance from the reservoir to the subjected area is long,
 316 possible frazil deposition could occur at the underside of ice floes. This is why the resistance for the
 317 single layer was increased from the default value to $n_i = 0.025 \text{ s} \cdot \text{m}^{-1/3}$. The Manning's roughness
 318 coefficients for ice jam was set to be identical for both sites ($n_i = 0.06 \text{ s} \cdot \text{m}^{-1/3}$). The initial ice
 319 thickness was used as 30 cm for both rivers based on the Institute of Meteorology and Water
 320 Management – National Research Institute (IMWM–NRI).

321 The group of parameters for Ice concentration were set to default values, which were set as 1.0 for
 322 static ice, 0.9 for surface frazil and 0.6 for ice rubble and floes accumulation. The value of the
 323 maximum concentration for ice rubble (0.6) is based on the assumption that ice jam has a porosity of
 324 0.4 (Prowse, 1990). This value was calibrated by means of the physical model study (Tuthill et al.,
 325 2008, 2008) and data from the historical ice jams, .i.e., the Thames River (Kolerski et al., 2016) and
 326 the St John River (Knack and Shen, 2016).

327 The stoppage criteria is a model parameter, which is responsible for artificially stopping the ice. This
 328 situation happens if the ice moves slowly, possibly attaching to other ice pieces or the border ice. At
 329 the aim of not considering any artificial stoppage or subjectively controlled ice jamming, this
 330 parameter was set to zero.

331 **Table 1. Calibrated parameters in the Odra and the Vistula Rivers. Parameters expected values available are referenced**
 332 **to literatures.**

Parameter	Unit	Value calibrated for the Odra	Value calibrated for the Vistula	Reference literature (if applicable)
Manning's roughness coefficient for single layer ice	$[\text{s} \cdot \text{m}^{-1/3}]$	0.025	0.02	(Ashton, 1986)
Manning's roughness coefficient for ice jam	$[\text{s} \cdot \text{m}^{-1/3}]$	0.06	0.06	(Ashton, 1986)
Initial ice thickens	[m]	0.3	0.3	
Ice internal friction angle	[°]	46	46	(Lal and Shen, 1991)

Wind-ice stress coefficient	[–]	0.0015	0.0015	(Wu, 1973)
Maximum concentration of ice parcels in jam	[–]	0.6	0.6	(Prowse, 1990)
Maximum concentration for skim ice and border ice formation	[–]	1.0	1.0	(Lal and Shen, 1991; Timalsina et al., 2013)
Maximum concentration for frazil ice	[–]	0.9	0.9	(Schneck et al., 2019)
Stoppage criteria for ice	[m · s ⁻¹]	0	0	
Total number of nodes in the domain	[–]	11311	22598	
Initial parcel size (for SPH calculation)	[m]	25	30	

333

334 1.3.2 Boundary conditions

335 1.3.2.1 Odra river

336 Boundary conditions related to river hydrodynamic were set to represent the flow conditions

337 observed during winter months. The data from Słubice gauging station were analyzed, where the

338 daily water surface elevation is recorded. The water discharge is also provided for the Słubice station.

339 In addition, the station has some ice thickness observations; however, this is mostly qualitative

340 information on the ice type (Wolski et al., 2017; Marszelewski and Pawłowski, 2019). Since detailed

341 ice conditions for the Lower Odra River are not known, the input data for the model were set at the

342 upstream boundary for an initial ice floe thickness of 0.3 m. The calculations do not include any

343 border ice, nor do they consider existing ice cover in the river. Thus, it was assumed that the river is

344 free of ice, and is subjected to possible ice jamming from breakup ice transported from upstream.

345 The data from 11 years of water discharge recorded at Słubice gauging station were analyzed to

346 estimate flow conditions for modeling. Data were provided by the hydrologic surveillance service of

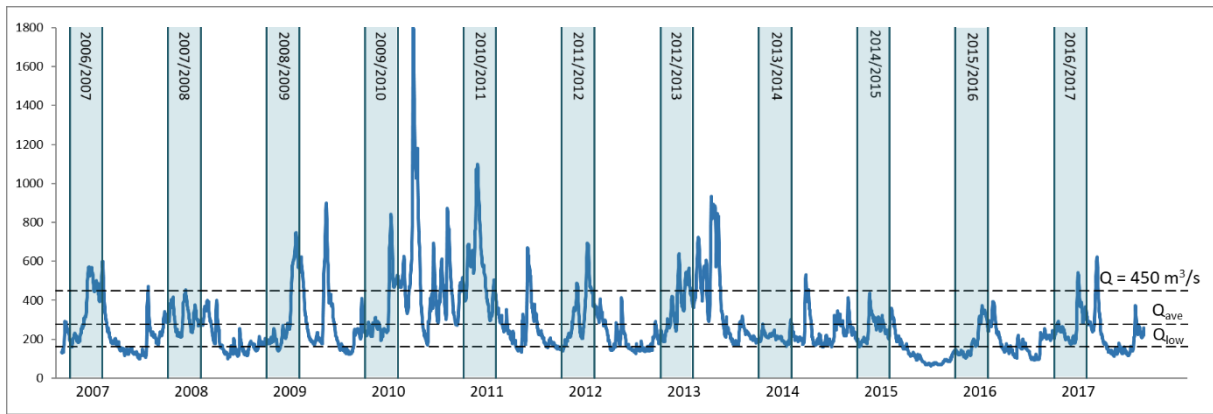
347 the Institute of Meteorology and Water Management – National Research Institute (IMWM–NRI).

348 Also, for the current study, the data were retrieved from < <https://dane.imgw.pl/> >. In Poland, the

349 water year is used for hydrological statistics; thus, the time series starts on 1st November, 2006 and

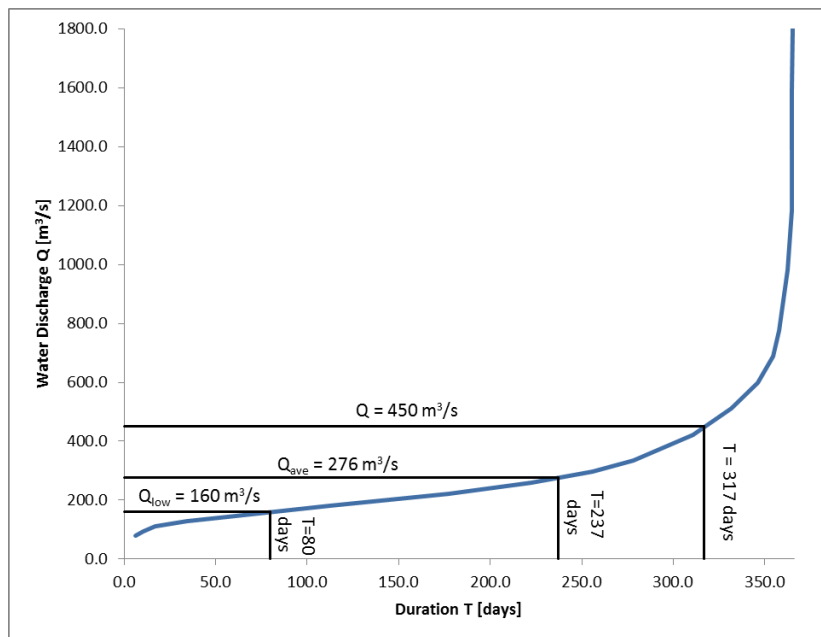
350 ending on 31st October, 2017 was used for the study. The more recent data was not available at the

351 time of conducting the study. The raw flow data is presented in Figure 9, and the discharge - time
 352 duration plot for an average year in Figure 10. The winter season was indicated in Figure 9 by
 353 marking the time with blue color (1st December – 31st March) .



354

355 **Figure 9** Water discharge at Słubice gauging station; winter seasons were marked with blue, and characteristic flows
 356 designated by dashed lines (data from <https://dane.imgw.pl/>)



357

358 **Figure 10** Water discharge duration for an average year at Słubice gauging station; flows used in the study and their
 359 durations were marked with black lines (data from <https://dane.imgw.pl/>)

360 The study considered three water discharge conditions: namely, yearly-average flow by $Q_{ave} = 276$
 361 m^3/s (based on the 10-year daily average data), low flow by $Q_{low} = 160 m^3/s$, and flow referring to the
 362 breakup condition $Q = 450 m^3/s$. Typically for the beginning of the winter season, the flow in the
 363 Odra River is reduced below the average flow, however rarely dropping to the low flow range. In

364 recent years, the only exception was the 2015/16 season, which was affected by extreme drought in
365 the summer season (Staśko and Buczyński, 2018). In consequence, during the entire winter season,
366 low water levels and discharge were observed.

367 The so-called 'typical breakup conditions' for Słubice ($Q = 450 \text{ m}^3/\text{s}$) refers to the average flow from
368 March. It is also the flow recorded on 27th February, 2010 during the mid-winter breakup, when the
369 case of an ice jam in Słubice developed due to the ice sluicing. In many years, in the second half of
370 the winter, the water discharge rose due to increased air temperature and melting snow, as well as
371 ice breakup. Recently, an increased discharge is more common for mid-winter, which is caused by
372 the changing long-term state of the atmosphere in the region. As a result, a mid-winter breakup may
373 occur leading to a potential ice jamming. Due to the frequency occurrence of the mentioned
374 circumstances, they were included in the simulations.

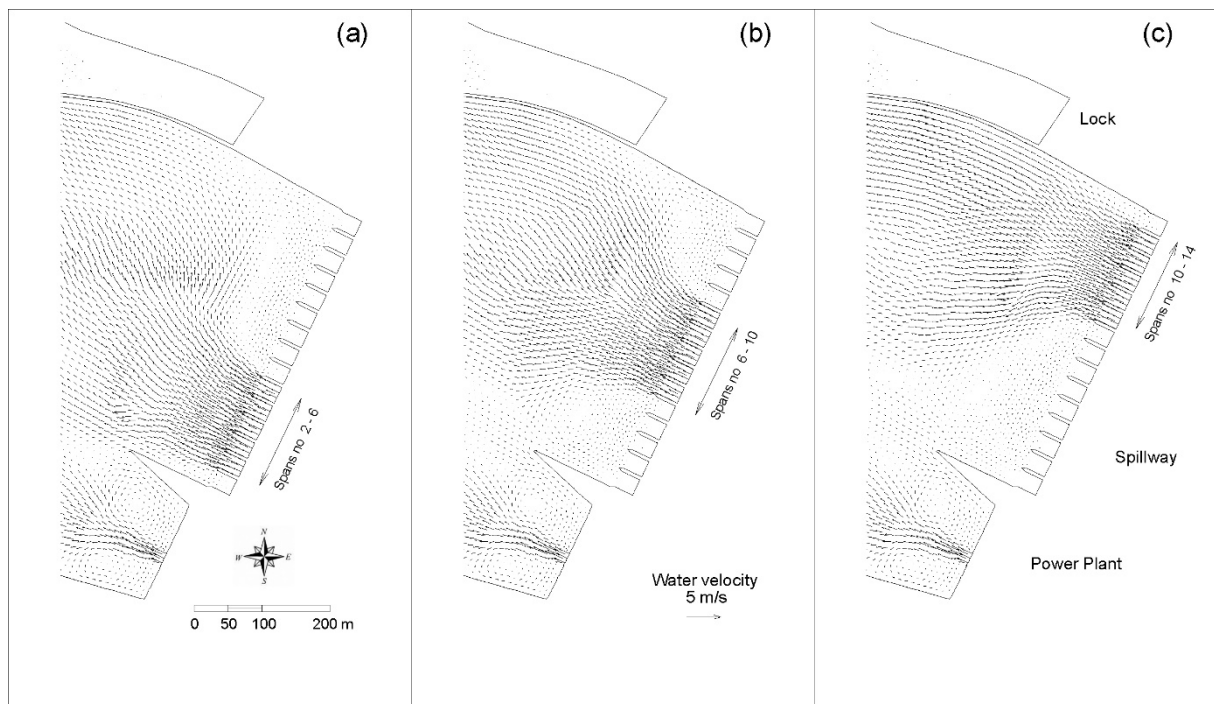
375 **1.3.2.2 Vistula river**

376 The upstream open boundary conditions were set at the cross-section of the existing Włocławek
377 diversion dam, in such a way that the dominant part of the flow was conveyed through the spillway,
378 and the rest through the power plant. The flow distribution was set according to the operation
379 procedure during ice sluicing, which is published yearly by RWMA Warszawa (RWMA, 2009). At the
380 downstream end of the model located at the proposed Siarzewo dam, the constant water surface
381 elevation was set up according to the proposed normal pool level. In addition, the outflow
382 boundaries were set at the proposed hydropower plant and the bypass channel. The downstream
383 open boundaries for water were assumed in the nodes located in each spillway section, at the
384 turbine outlets and the bypass channel (fish passage inlet). It was considered for setting the ice
385 boundary condition that ice sluices solely through the spillway.

386 The following calculation conditional variants, from the hydrodynamics point of view, were carried
387 out for the numerical analysis: average flow $Q_{\text{ave}} = 924 \text{ m}^3/\text{s}$ and discharge of 1308, 3008, 4538 and
388 $6104 \text{ m}^3/\text{s}$. As an example, the boundary conditions for water discharge $Q = 924 \text{ m}^3/\text{s}$ are shown in



389 figure 8 and 11. At the upstream flow boundary, the proportions were set as 724 m³/s in the spillway
 390 and 200 m³/s in the power plant (see Figure 8). At the model downstream, both the water surface
 391 elevation and discharge conditions were used. Water discharge was set at two locations: the inlets to
 392 the power plant and the entrance to the bypass channel, while the water surface elevation
 393 conditions were used at the spillway. The constant water level of H = 46 m a.s.l. was used, which is
 394 the equivalent of the normal pool level at the proposed reservoir. Water discharge was set up for the
 395 value of 200 m³/s through the hydropower plant (carried out through one of seven turbines, no 4,
 396 counted from the left bank). In addition, the water flow of 20 m³/s was conveyed through the bypass
 397 channel. The remaining part was distributed over 5 out of 15 spans of the spillway, but no specific
 398 value for the discharge was used due to the WSE boundary conditions applied at the spillway. Three
 399 spillway opening setups were tested (as shown in Figure 11), assuming the spans in the immediate
 400 vicinity of the power plant (span no 1) and the lock (no 15) always being closed.



401
 402 **Figure 11 Siarzewo spillway opening systems used for calculations at a flow of 924 m³/s, open spans from 2 to 6 (a), open**
 403 **spans from 6 to 10 (b) and open spans from 10 to 14 (c); Note, the river section shown in the figures is downstream of**
 404 **the proposed dam and is not included in the current simulations**



405 All numerical simulations were carried out with and without taking into account the wind action. For
 406 those cases applied under the wind effect influence, the wind blows from the west, north, east and
 407 south with a speed of 3 m/s for average flow conditions, and 4 m/s for all other simulated cases. The
 408 reduced wind speed for average water flow was based on the fact that the ice was not able to run
 409 downstream of the reservoir, drifting towards the banks (for the wind velocity of 4 m/s).

410 **Table 2. Scenarios proceeded for the Vistula River study**

Case no	Water discharge	Spillway opening spans from left	Wind	
			Speed	Direction
[-]	m ³ /s	[-]	[m/s]	[-]
1	Q = 924 m ³ /s	0xxxxx000000000*	0	No wind
2			3	W ⇒
3			3	S ↑
4			3	E ⇐
5			3	N ↓
6		000000000xxxxx0	0	No wind
7			3	W ⇒
8			3	S ↑
9			3	E ⇐
10			3	N ↓
11		00000xxxxx00000	0	No wind
12			3	W ⇒
13			3	S ↑
14			3	E ⇐
15			3	N ↓
16	Q = 1308 m ³ /s	0xxxxxxxx000000	0	No wind
17			4	W ⇒
18			4	S ↑
19			4	E ⇐
20			4	N ↓
21		000000xxxxxxxx0	0	No wind
22			4	W ⇒
23			4	S ↑
24			4	E ⇐
25			4	N ↓
26	Q=3008 m ³ /s	0xxxxxxxxxx0000	0	No wind
27			4	W ⇒
28			4	S ↑
29			4	E ⇐
30			4	N ↓
31		0000xxxxxxxxxx0	0	No wind
32			4	W ⇒
33			4	S ↑
34			4	E ⇐
35			4	N ↓
36	Q = 4538 m ³ /s	0xxxxxxxxxxxxx0	0	No wind
37			4	W ⇒
38			4	S ↑
39			4	E ⇐

40			4	N ↓
41	Q = 6104 m ³ /s	0xxxxxxxxxxxx0	0	No wind
42			4	W ⇒
43			4	S ↑
44			4	E ⇐
45			4	N ↓

411 *) 0 – closed; x – open

412 In total, 45 number of simulations were made. The initial ice thickness was established at 0.3 m and
413 the ice was discharged through a spillway with an initial concentration of 0.4 for all analyzed cases.
414 This means that at the upstream boundary conditions, a 0.3 m thick ice inflow with a surface
415 concentration of 0.4 was implemented over the entire time of the simulation. It should be noted
416 that the maximum permissible ice jam concentration in the DynaRICE model is 0.6, and a further
417 increase in the concentration leads to an increase in jam thickness. Due to the protection of the inlet
418 to the hydroelectric power plant against incoming ice, in all simulations, it was assumed that the ice
419 cover remained intact on the right bank of the reservoir for a distance of about 2 km upstream of the
420 dam, overlapping with the dredged area shown in Figure 6.

421 1.4 Methodology

422 The process of locally reduced conveyance of ice transport resultant from channel narrowness, in the
423 case of a continuous ice inflow from upstream, often initiates an ice jam. Over time, it will lead to an
424 increase in the ice thickness and a constriction of the river cross-section, which results in the
425 impeded water outflow and an increase in water surface elevation in the section upstream of the
426 jam. This process is well known and described in the literature (Beltaos, 1995; Shen et al., 2008;
427 Pawłowski, 2019) as a phenomenon responsible for ice jam processes on rivers. For the estimation of
428 the congestion potential of a selected location on a river, both the following factors, ice velocity and
429 ice thickness change in time; thereby must be taken into account as indicators. This method for the
430 estimation of the jam potential was used in the past (i.e. (Knack and Shen, 2017; Shen et al., 2005));
431 however, for the purpose of this study, a modified procedure was proposed. The current method is
432 taking into account the change in the ice velocity in relation to the water velocity, and the increase in
433 the ice thickness in relation to the initial thickness of a single ice floe. This criteria is only applicable

434 for the break-up ice jam conditions without considering the thermal effect on the ice run. Thermal
 435 processes could change proposed thresholds.

436 Four criteria for assessing ice jamming were adopted: (0) no jam, (1) jam possible, (2) jam probable,
 437 (3) ice jam. No ice jam implies that ice is proceeding without stop, and neither increased thickness
 438 nor reduction of the ice velocity is projected. Jam conditions (1) and (2) refer to some reduction in
 439 the ice velocity, as well as an increase in the surface ice concentration. The possible jam condition (1)
 440 indicates increased ice concentration due to a reduction in ice velocity, leading to some thickening of
 441 ice. Using the above criterion, an analysis of the jam potential of the two Polish rivers was carried
 442 out: the Vistula River, at the upstream of the planned Siarzewo diversion dam, and the Odra River in
 443 the Słubice region after the modernization of the river training structures. All threshold conditions
 444 are summarized in Table 3.

445 **Table 3. Conditions used in the study to determine the jam potential for the numerical model results**

Jam potential	$\frac{\text{Ice velocity } (V_i)}{\text{Water velocity } (V_w)}$	$\frac{\text{Ice thickness } (\eta_i)}{\text{Single floe thickness } (\eta_0)}$
(0) No jam	>0.9	<1.1
(1) Jam possible	0.9 – 0.5	1.1 – 2.0
(2) Jam probable	0.5 – 0.15	2.0 – 3.0
(3) Ice jam	< 0.15	> 3.0

446

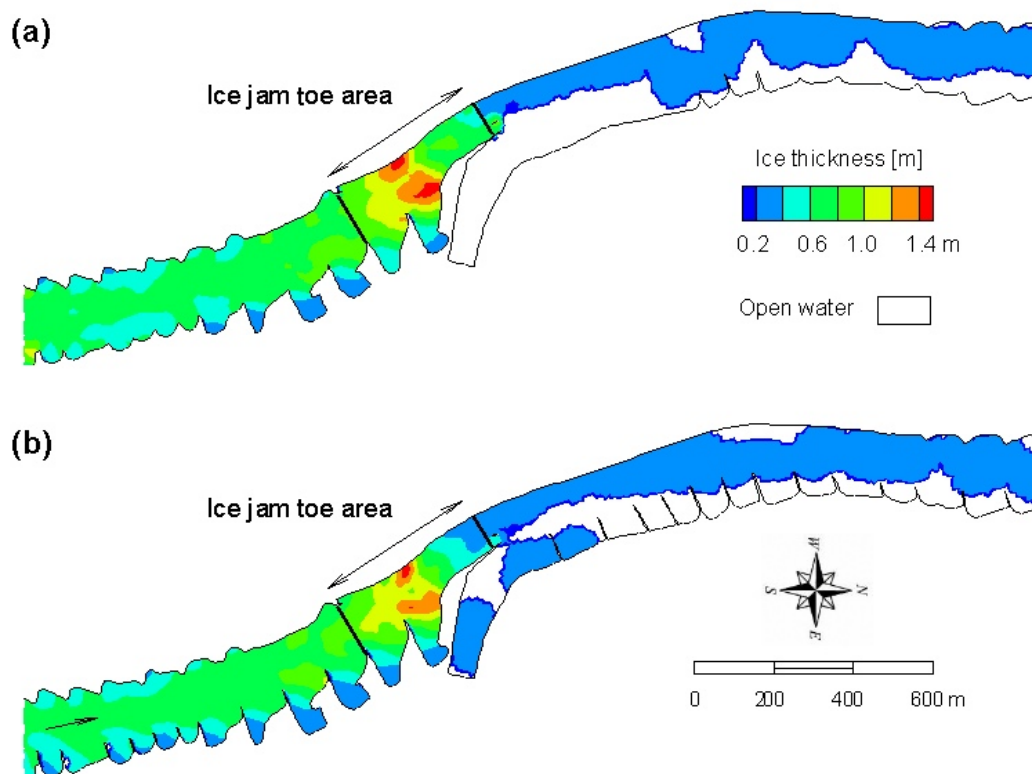
447 Once the calibrated mathematical model is implemented in the selected areas, the numerical
 448 simulations can be processed, and the obtained results must be analyzed in terms of ice
 449 accumulation and jamming.

450 **2 Results and discussion**

451 **2.1 Odra River**

452 To check the ice conditions in the vicinity of the Słubice-Frankfurt Bridge, a mathematical model was
453 applied to a 5 km longitudinal section of the Odra River. Probable ice jam conditions represent the
454 case in which the increased ice thickness is more than 2 times the initial ice thickness. Also, in this
455 case, the area-averaged ice velocity in an initially specified location drops below 50% of the average
456 water velocity in that area. Ice jam conditions are defined by a further velocity reduction to 15% of
457 the water velocity, and the ice thickness increasing to 3 times the initial, single ice floe thickness.

458 The results showed a consistent trend over the time; although, the results from the last hour are
459 discussed in this study. For the low flow, ice transport through the bridge cross-section is hampered
460 and the ice accumulation is observed. A comparison of the ice thickness distribution for high ice
461 inflow ($Q_i/Q_w = 0.048$) is presented in Figure 12 in the form of a contour plot of the 24th hour of
462 simulation. It shows increased ice thickness upstream of the bridge cross-section. The cause of such a
463 formation is ice congestion since the ice transport is severely hindered by the reduced cross-section.
464 In this hydrodynamic condition, the reconstructed river training structures affected the ice transport
465 insignificantly.

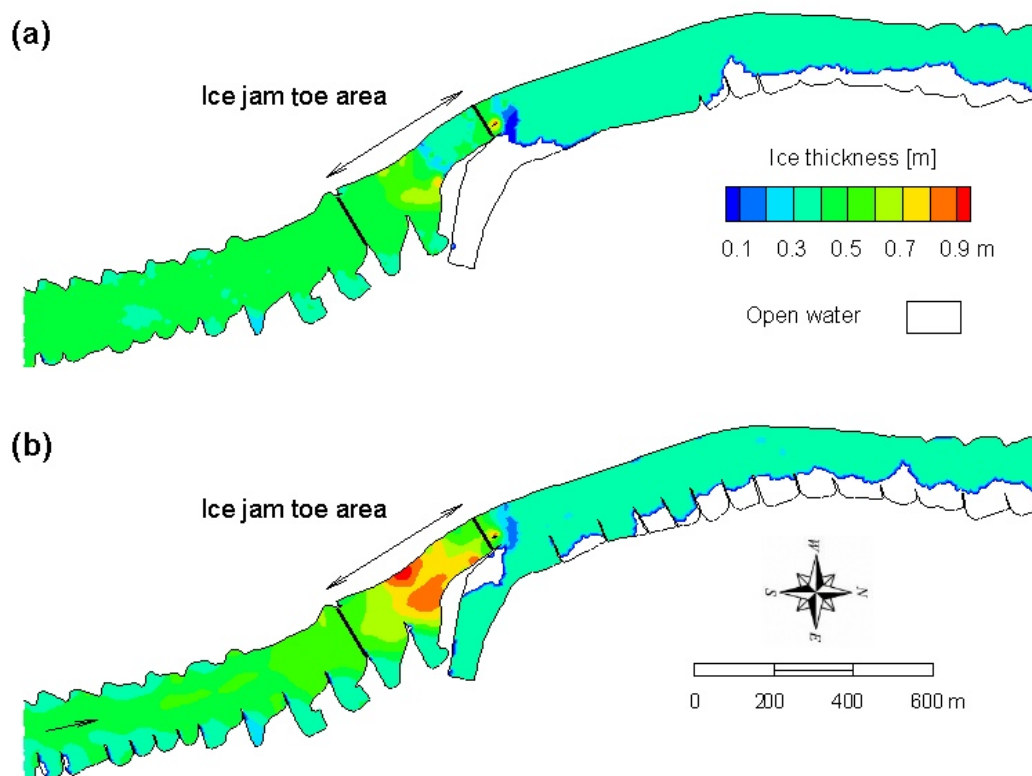


466

467

468

Figure 12 Simulation results of ice thickness at low flow ($Q_w = 160 \text{ m}^3/\text{s}$) and high ice inflow ($Q_i/Q_w = 0.045$) for current (a) and proposed (b) conditions; sub-domain for numerical jam analysis designated by black lines



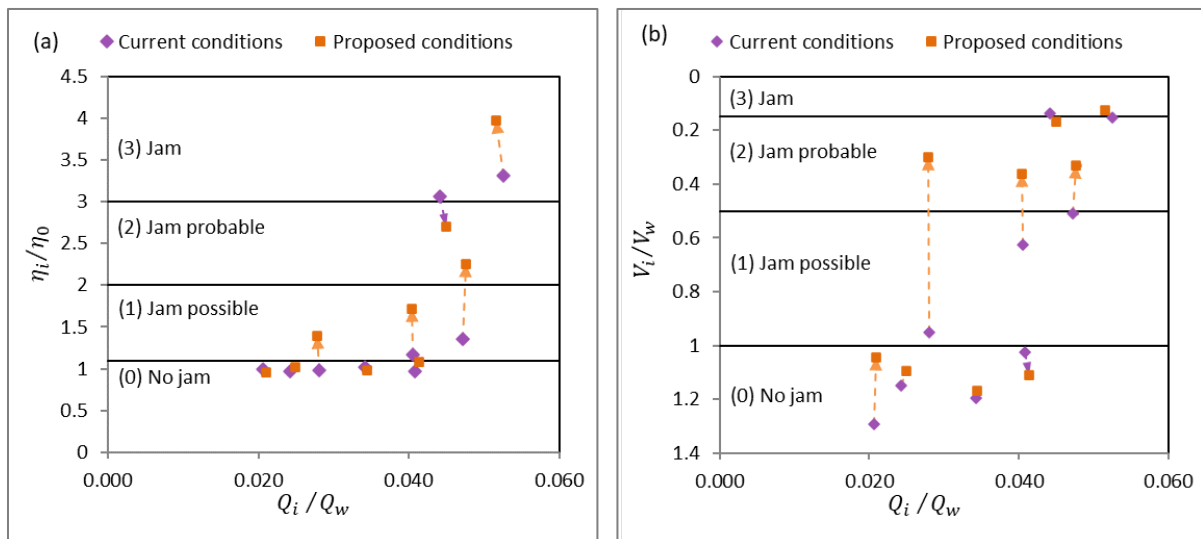
469
 470 **Figure 13. Simulation results of ice thickness at average flow ($Q_w = 276 \text{ m}^3/\text{s}$) and high ice inflow ($Q_i/Q_w = 0.048$) for**
 471 **current (a) and proposed (b) conditions; sub-domain for numerical jam analysis designated by black lines**

472 The results for average flow showed , the proposed structures reduced the river capacity for ice
 473 transport. Since the constant ice concentration is applied as the upstream boundary condition,
 474 different magnitude of water discharge changes the amount of the ice inflow and the resulting ice
 475 volume in the domain. Three cases of different ice inflow were simulated and all the calculation
 476 results with the proposed structures led to a larger ice accumulation in comparison to the current
 477 conditions. The final results of the case with average flow ($Q_w = 276 \text{ m}^3/\text{s}$) and high ice discharge
 478 ($Q_i/Q_w = 0.048$) are shown in Figure 13.

479 All simulation results with high water discharge ($Q_w = 450 \text{ m}^3/\text{s}$) showed that ice is transported
 480 downstream, without stoppage. Only, is some insignificant shore accumulations perceptible for both
 481 the current and proposed regulating structures. Thus, the ice thickness distribution over the model
 482 domain is not presented in this domain. It is mainly caused by the low ice-to-water discharge ratio,



483 and high drag force from the increased water velocity. Consequently, ice is less prone to a stop and
 484 the release of any form of the accumulation would be facilitated by the high water drag force.



485

486 **Figure 14** Numerical simulation results of ice jamming for the Słubice according to ice thickness increase (a) and ice velocity
 487 reduction criterion (b); purple and orange clusters refer to current and proposed conditions, respectively

488 The simulation results are summarized in Figure 14 and Table 4, showing the ice jam potential for the
 489 aforementioned location. The analysis includes a wide variation of water and ice discharge, covering
 490 the conditions typical for winter months which are low or average flow. It also includes the condition
 491 which is common for breakup condition, and represented by flow above average with increased ice
 492 discharge. The numerical model results show, for most cases the ice run is hampered by new
 493 structures. The extension of the spurs will act towards a flow constriction and velocity increase in the
 494 main channel. However, in the vicinity of the bridge, the cross-section will be reduced by the newly
 495 designed structures. As a consequence, the congestion of the ice is observed due to the convergence
 496 of the flow. In addition, at the upstream of the river, the regulation increase the ice supply to the ice
 497 congestion area.

498 The influence of river regulation is particularly visible for the case of low water discharge ($Q_w = 160$
 499 m^3/s and low ice inflow of $Q_i/Q_w = 0.028$). In such case, the new structures put a stop to the ice
 500 run. Simulation results show the reduction of the ice velocity to not more than 30% of the water
 501 velocity. However, due to the low flow in line with low water velocities, this case did not show a

502 significant increase in the thickness of the ice ($\eta_i/\eta_0 = 1.39$). It can be concluded that, from the two
 503 mentioned criterion, the velocity ratio is more likely to predict jamming. Since this study mostly
 504 concerns the low flow condition, in the case of ice blockage, water velocity is not high enough to
 505 develop thick ice jam toe. As a result, ice stoppage is more commonly evident than the increase of
 506 the ice thickness.

507 **Table 4. Numerical simulation results for the Odra river, Stubice station**

Model input; upstream boundary			Model results averaged over the sub-domain					Conditions
Water Discharge Q_w	Ice discharge Q_w	$\frac{Q_i}{Q_w}$	Ice thickness η_i	Ice velocity V_i	Water velocity V_w	$\frac{\eta_i}{\eta_0}$	$\frac{V_i}{V_w}$	
[m ³ /s]	[m ³ /s]	[m ³ /s]	[m]	[m/s]	[m/s]	[-]	[-]	C/P*
160	4.5	0.028	0.30	0.57	0.60	0.99	0.95	C
	4.5	0.028	0.42	0.17	0.55	1.39	0.30	P
	7.1	0.044	0.92	0.09	0.69	3.06	0.14	C
	7.2	0.045	0.81	0.10	0.60	2.70	0.17	P
	8.4	0.053	0.99	0.11	0.71	3.31	0.15	C
	8.2	0.052	1.19	0.08	0.68	3.97	0.13	P
276	11.2	0.041	0.35	0.60	0.96	1.17	0.62	C
	11.1	0.040	0.52	0.32	0.89	1.72	0.36	P
	6.7	0.024	0.29	1.08	0.94	0.97	1.15	C
	6.9	0.025	0.31	0.94	0.85	1.02	1.10	P
	13.0	0.047	0.41	0.49	0.96	1.36	0.51	C
	13.1	0.048	0.68	0.30	0.91	2.26	0.33	P
450	15.4	0.034	0.31	1.66	1.39	1.02	1.20	C
	15.5	0.034	0.29	1.47	1.26	0.98	1.17	P
	9.3	0.021	0.30	1.68	1.30	1.00	1.29	C
	9.4	0.021	0.29	1.29	1.24	0.96	1.04	P
	18.4	0.041	0.29	1.46	1.42	0.96	1.03	C
	18.6	0.041	0.33	1.37	1.23	1.09	1.11	P

508 *C – current conditions; P – proposed conditions

509 The simulation result indicates, although, spur dikes can increase the ice jam potential, they regulate
 510 the river by producing backwater effect. Because of the reduction in the cross section width, the
 511 water level increases. Since the increased depth can be considered as an advantage for the ice
 512 breakers to not be stuck in the shallow areas, mechanical ice breaking (with the advantage of ice
 513 breakers) is the proper approach in this circumstance. Therefore, both river regulation and increase
 514 in the water level provided by presented spur dikes will mitigate the ice jam related condition.

515 **2.2 Vistula River**

516 According to the obtained numerical model results, two areas of potential ice jamming were selected
517 in the reservoir: the bridge cross-section and the downstream area where the proposed islands are
518 designed. Both areas, as indicated in Figure 6, were considered for further analysis within the
519 proposed methodology. The results are presented in Table 5 (upstream location) and Table 6
520 (location in the vicinity of the dam) for selected cases.

521 In the first mentioned location, which is a short distance downstream of the existing dam
522 (679+200 river km, about 4.5 km), the piers of the bridge hinder the ice run. This is particularly likely
523 in the event of low water flow and high ice concentration. Ice sluicing through the proposed dam
524 shall not be performed if the water discharge does not reach the average flow conditions; therefore,
525 low flow scenarios were not performed. Among all the calculated cases, the greatest risk of ice
526 jamming is observed for simulations with average flow ($Q_{ave} = 924 \text{ m}^3/\text{s}$), and wind blowing from the
527 opposite direction to the water flow.

528 Under these conditions, the bridge opening (horizontal distance between two piers) is not sufficient
529 to allow a continuous run of ice of high concentration. This leads to ice congestion and stop near the
530 bridge piers in the central part of the river, which retards the ice movement, and in some locations,
531 the formation and progression of the juxtaposed ice cover in an upstream direction. The process
532 becomes more dynamic once the ice cover progression reaches the vicinity of 677 river km. In that
533 section, the river originally meandered between alluvial islands on both banks; even though, due to
534 the formation of the reservoir, the islands were inundated forming shoals hindering the ice run. It led
535 to additional stops, and accelerated the accumulation of inflowing ice and eventual jam formation.
536 For average flow conditions, ice was sluiced through 5 out of 15 spillway spans, and three
537 configurations of spillway opening were tested. However, this has no effect on the ice dynamic in the
538 upstream section of the reservoir.



539 Some effects were also observed for the discharge $Q = 1308 \text{ m}^3/\text{s}$; however, in this case, it was only a
 540 local retardation of the ice movement and a negligible increase in the ice thickness at the upstream
 541 face of the bridge piers. While continuing the simulation, the process did not develop nor progress
 542 towards the upstream with time. For cases with a higher flow discharge, the water drag was
 543 sufficient to release any ice stop at the bridge cross-section and ice transport proceeded smoothly
 544 towards the downstream. Thus only cases with average discharge were considered for further testing
 545 within the proposed procedure. All simulation results are presented in Table 5 and also presented in
 546 a form of contour plot of the ice thickness in Figure 15.

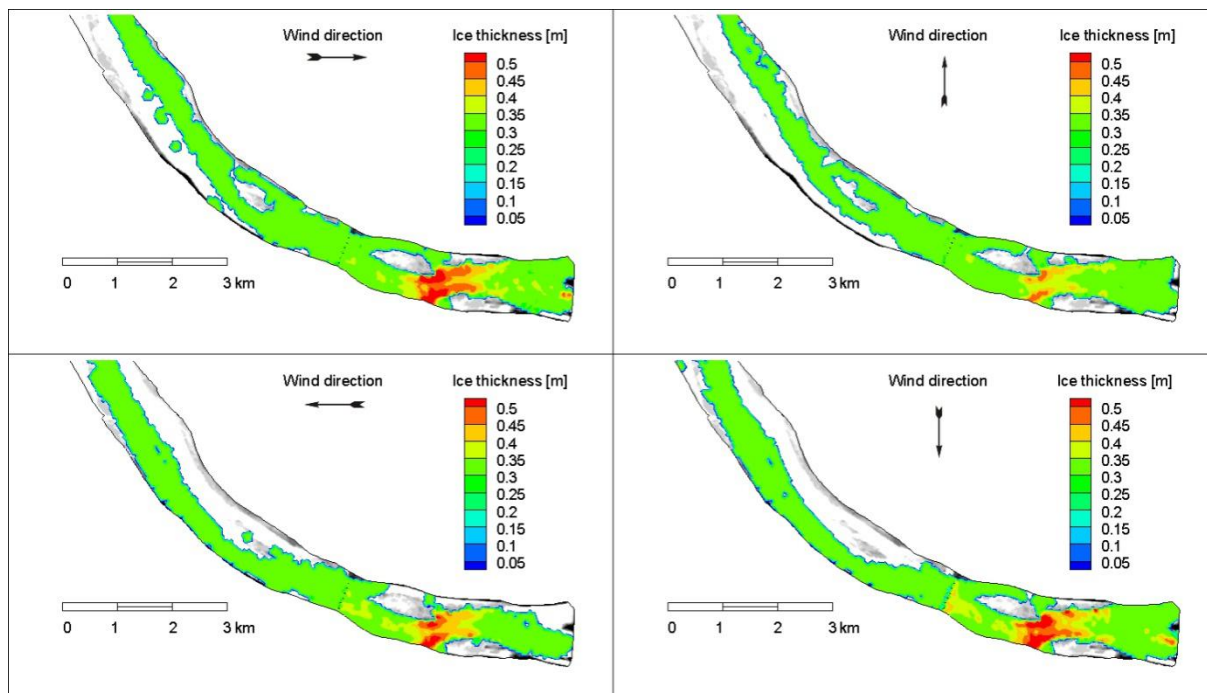
547 The second location where ice jamming was observed is the area close to the proposed dam (701 - 703
 548 river km). The calculations carried out for the average flow and a flow of $1308 \text{ m}^3/\text{s}$ clearly show that,
 549 the locations of the mentioned artificial islands should be reconsidered, and the change in the layout
 550 of the southernmost island of the group is absolutely necessary. The southern front of the southern
 551 island (around 702+650 river km) is a place wherein due to the event of a wind blowing from the north
 552 and west, ice accumulation and potential ice jamming can occur. A change in the shape of the southern
 553 shore of the island should be considered to direct ice towards the spillway. For the higher flow velocity
 554 conditions, the water drag is high enough to push ice towards the spillway without any significant ice
 555 stop. Also, for the higher discharges, the ice flows in the shallow channel between the islands and the
 556 bank. The results of numerical modeling also indicated a significant force, exceeding 2 kN/m^2 , to be
 557 transferred from the ice to the shore of the artificial islands. This force must be withstood by the
 558 islands' borders; although, considering the purpose of the islands, neither riprap nor concrete could
 559 be used to reinforce the shores.

560 **Table 5. Simulation cases and obtained results for the Vistula River study for the water discharge $Q = 924 \text{ m}^3/\text{s}$ and single**
 561 **floe thickness $\eta_0 = 0.3 \text{ m}$; area at the upstream of the reservoir (677 – 678 river km)**

Case no	Water	Ice	Spillway opening spans from left	Wind		Ice thickness (η_L)	Average velocity		$\frac{(V_i)}{(V_w)}$	$\frac{(\eta_i)}{(\eta_0)}$
	Discharge	discharge		speed	direction		Ice (V_i)	Water (V_w)		
	[m^3/s]	[m^3/s]	[-]	[m/s]	[-]	[m]	[m/s]	[m/s]	[-]	[-]
39		12.3	00000xxxxx00000*	3	No wind	0.41	0.072	0.246	0.29	1.36

40	Q = 924 m ³ /s	12.2		3	W ⇒	0.47	0.068	0.236	0.29	1.58
41		12.1		3	S ↑	0.399	0.060	0.244	0.25	1.33
42		12.2		3	E ⇐	0.44	0.078	0.247	0.32	1.48
43		12.2		3	N ↓	0.47	0.069	0.243	0.28	1.57

562 *) 0 – closed; x – open



563

564 **Figure 15** Ice thickness distribution in the upstream part of the proposed reservoir for the average discharge $Q_{ave} = 924$
565 m^3/s and varying wind direction at a speed of 3 m/s

566 Recently, before the new dam construction, some ice stops has been observed upstream of the
567 bridge, as a result of ice sluicing from Włocławek spillway. The inflow to the new reservoir considers
568 to be the outflow from the existing reservoir, which forms the upstream open boundary for the
569 current model. Concerning the procedure of the icebreaking operation on Włocławek reservoir, the
570 competent Water Authority should allow ice sluicing only if ice jamming on the reservoir is observed,
571 or if a significant amount of ice is released in the river upstream of the reservoir. If the above-
572 mentioned conditions occur, it is still not recommended to release ice for a water discharge below
573 $1308 m^3/s$. Thus, simulated cases with average water flow should be considered as worst-case
574 scenarios, occurring only in very unusual conditions.

575 The simulation results indicate the strong effect of the river bathymetry on the ice transport,
576 compounded by the presence of the bridge piers and wind. At first, the ice cover develops upstream
577 of the bridge piers. During the time, the progressing ice cover in addition to the restriction at the
578 cross sections out of the existing islands, lead to an increase in the ice jam formation upstream of the
579 piers. That is mainly due to the fact that, at the restricted area between the islands, the water
580 velocity is increased (thereby, drag force of water rises), causing higher velocity for the ice run.
581 Entering the ice stoppage area, the ice particles become a part of the ice jam due to the ice
582 resistance force. As shown in Figure 15, all cases with average flow, where the two islands are
583 located and river meanders, show ice accumulation on both banks . After the reservoir is formed, the
584 water level will increase to the normal pool level. However, the most parts of the upstream section
585 of the proposed reservoir will preserve their river-like character, and the main currents will follow
586 the thalweg. According to the numerical results shown in Table 5, all cases with average flow will
587 cause a reduction in the ice velocity in comparison to the water velocity by more than 70%, except
588 for the case with an eastern wind. In this case, the wind accelerates the ice movement; although, due
589 to the existence of the bridge piers, ice flow converges and ice transport becomes limited, leading to
590 the ice accumulation in the upstream. Considering ice-to-water velocity conditions, all cases with
591 average flow represent a strong possibility of ice jam formation.

592 The increase in the ice thickness is variable from case to case, and in all five simulated cases, the
593 most severe conditions are expected for the case with the western and northern wind. In both
594 mentioned cases, wind pushes the ice in an opposite direction to the flow or towards the outer bank.
595 This causes additional resistance to the ice due to the contact between the ice and the banks. In
596 consequence, the ice increases in thickness by roughly 60 %, being classified as 'ice jam probable'
597 type in both cases. Other cases similarly indicate increased ice thickness; although this growth
598 appears to be to a lesser extent, thusly being classified as 'ice jam possible' type.

599 The second area where ice jam potential was tested is within a distance of 4 km in the upstream
 600 direction from the proposed dam (703 – 704 river km, see Figure 6). In this location, the water
 601 surface elevation is nearly horizontal due to the backwater effect, and the water velocity is relatively
 602 low (based on the high water depth). With regard to the force balance on movable ice, the drag force
 603 from water is not significant, hence the impact of additional obstacles on the ice run in this area may
 604 cause ice stop. The ice movement is affected by the artificial islands located along the outer bank of
 605 the reservoir, which causes a narrowness of the cross-section area by about 12%. The upstream
 606 shore of the southernmost island was designed in a non-streamlined shape, which significantly
 607 impedes the both ice and water flow.

608 Ice jamming in the downstream section of the reservoir is less located. However, due to the
 609 proximity of the dam, as well as the wind and flow impact on the ice dynamic, the effect of the
 610 spillway opening was considered. The ice jam potential upstream of the dam was determined for
 611 above average water discharge ($Q = 1308 \text{ m}^3/\text{s}$), with variable number of open spillway's spans and
 612 wind directions. For these hydrodynamic conditions, ice was supplied in the upstream of the model,
 613 with the surface ice concentration of $N = 0.4$. This value of concentration leads to the ice discharge
 614 varying from $13.3 \text{ m}^3/\text{s}$ to nearly $15 \text{ m}^3/\text{s}$ which is about 1% of the water discharge. Since the jam has
 615 no clear location of the toe, the averaged ice thickness was applied over the reach of about 2 km of
 616 the reservoir, upstream of the artificial islands. The same area was used at the aim of averaging out
 617 ice and water velocities, and all the results are summarized in the Table 6. The last two columns of
 618 the table are the relative ice-to-water velocity ratio and the increase in the ice cover thickness.

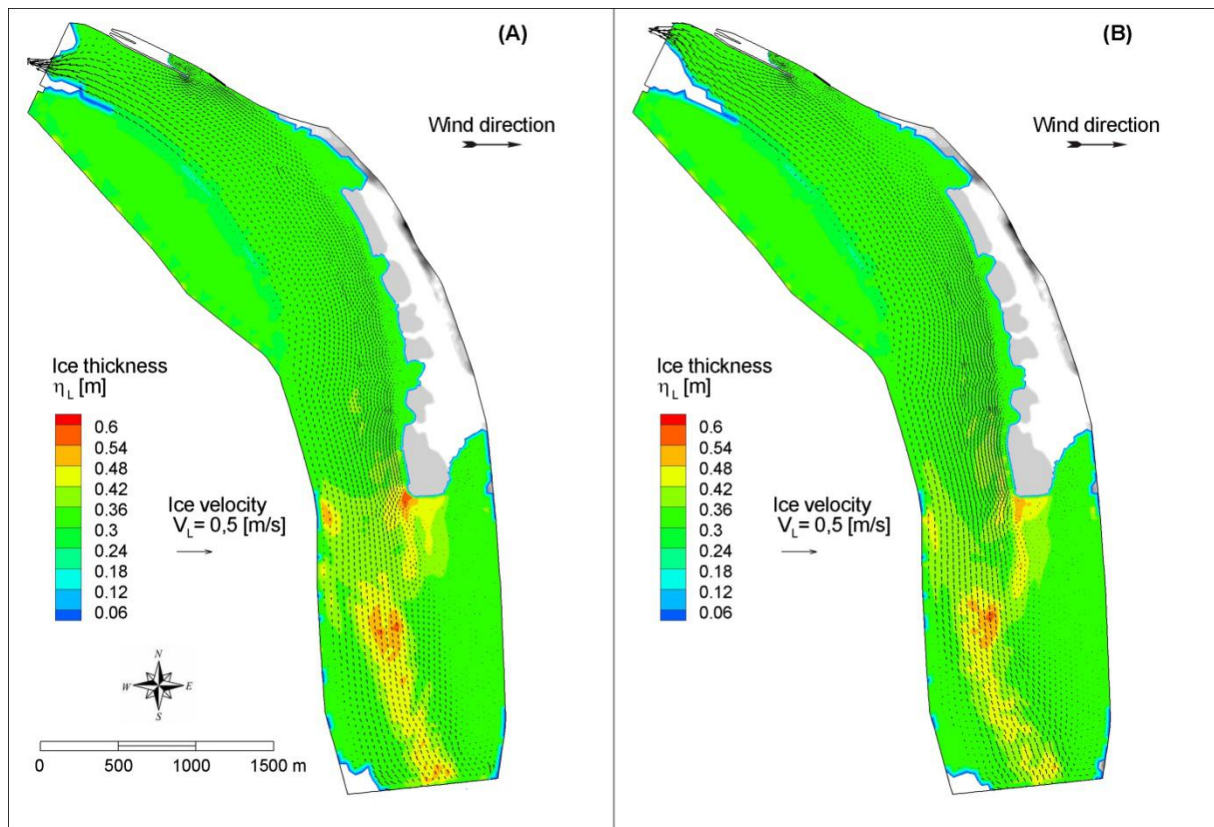
619 **Table 6. Simulated cases and obtained results for the Vistula River study with the water discharge of $Q = 1308 \text{ m}^3/\text{s}$ and**
 620 **the single floe thickness $\eta_0 = 0.3 \text{ m}$; area at the downstream of the reservoir (703 – 704 river km)**

Case no	Water	Ice	Spillway opening spans from left	Wind		Ice thickness (η_L)	Average velocity		$\frac{(V_i)}{(V_w)}$	$\frac{(\eta_i)}{(\eta_0)}$
	Discharge	discharge		speed	direction		Ice (V_i)	Water (V_w)		
	[m^3/s]	[m^3/s]	[-]	[m/s]	[-]	[m]	[m/s]	[m/s]	[-]	[-]
1	$Q = 1308$	13.4	0xxxxxxxx000000*	0	No wind	0.30	0.198	0.198	1.00	1.00
2		13.4		4	W \Rightarrow	0.37	0.023	0.169	0.13	1.23

3		13.3		4	S ↑	0.30	0.286	0.189	1.51	1.00
4		14.9		4	E ←	0.31	0.113	0.230	0.49	1.01
5		15.0		4	N ↓	0.35	0.024	0.172	0.14	1.16
6		13.3		0	No wind	0.34	0.040	0.170	0.24	1.12
7		13.5		4	W ⇒	0.424	0.017	0.171	0.10	1.41
8		13.3	000000xxxxxxxx0	4	S ↑	0.30	0.289	0.190	1.52	1.00
9		13.4		4	E ←	0.30	0.277	0.244	1.13	1.00
10		13.3		4	N ↓	0.30	0.152	0.244	0.62	1.00

621 *) 0 – closed; x – open

622 The simulation results show the significant impact of the wind on ice jam formation. It is a logical
623 consequence of the backwater effect that causes an increase in depth and a decrease in water
624 velocity in the direct vicinity of the dam. In such conditions, the wind develops the main drag force
625 on the surface ice transport. Thus, while the wind is blowing in the same direction as that of the
626 water flow, it causes the ice to run with a speed exceeding the downstream water velocity. In such a
627 case, the ice is pushed towards the dam, and no ice stoppage is observed at the southern shore of
628 the island (see cases 3, 8 and 9 in the Table 6). This is clearly visible for a southern wind, but also for
629 an eastern one. However, in this case, the order of opening the spans of the spillway will have an
630 impact on the ice transport. Meanwhile, wind blowing from the opposite direction (west) to the
631 water flow leads to the ice stoppage and jamming (Figure 16). Due to the fact that the water drag is
632 not high, the accumulation is not very thick without a clear location of toe; however, the ice run
633 proceeds with low velocity ($V_i/V_w < 0.15$). Thus, the ice accumulation propagates upstream of the
634 reservoir; even though, it develops in a juxtaposed ice form due to the low water drag.



635

636 **Figure 16 Ice thickness and ice velocity distribution in the downstream area of the reservoir for the water discharge $Q =$**
 637 **$1308 \text{ m}^3/\text{s}$ and variable spillway span opening: left (a) and right spans (b)**

638 The abovementioned situation with the eastern wind, as well as the case with the northern wind are
 639 affected by the spillway operation. Even though, the distance from the spillway to the area of
 640 interest is about 4 kilometers, the reduction in ice sluicing caused by opening the wrong spillway
 641 sections enables ice accumulation to happen upstream. Since the water velocity at the reservoir is
 642 significantly reduced due to the backwater effect, the main mechanism affecting the ice flow at the
 643 direct vicinity of the spillway will be the wind. For an eastern wind, although intact ice covers the
 644 area on the left bank, ice drifts away from the opened sections of the spillway towards the west
 645 bank. Consequently, less ice will pass the dam, and its movement will be hampered in the entire
 646 reservoir. It was shown in Table 6 that the ice velocity is reduced, but the thickness did not increase
 647 from the single floe thickness. For this reason, it must be noted that the span opening configuration
 648 will mainly be determined by the ice dynamic in the reservoir and its inflow towards the spillway,
 649 together with the wind direction.

650 The ice jam commonly happens during the low flow condition that may not necessarily lead to the
651 risk of flooding due to the low discharge. However, in the case of not releasing the ice jam in the
652 warm spell of spring, increased discharge resultant from the snow melting may cause flooding
653 damages.

654 **3 Conclusion**

655 In determining the ice jam potential for rivers that are subjected to the extensive engineering works,
656 it is important to predict and eliminate possible risk (Shen, 2016). The proposed methodology,
657 because of the minimum user interference, excludes introspective errors. However, it does not
658 undermine the already existing practices. As shown by the examples, the obtained results clearly
659 determine and assess the potential ice jamming that arises from the proposed engineering works.
660 Considering the Odra River flood management project, the possibility of ice jam formation resulting
661 from the river engineering works in the Stubice area is increased if an ice run of high concentration
662 occurs during average flow conditions. While the risk of ice jamming during the low flow conditions is
663 reduced. It should also be noted that the formation of a main channel with a relatively uniform depth
664 will greatly enhance the ice-breaking operation. Although jams may form to a greater extent, they
665 will be easier to release. The application of the mathematical model to the proposed reservoir on the
666 Vistula River in the scope of the ice dynamics, has been a success, because it helped to deliver on two
667 very important targets: establishing frames for ice sluicing operations, and redeveloping the artificial
668 islands. Processing the numerical model results according to the presented methodology contributed
669 to the designation of areas prone to ice jamming and the level of the related risk assessment.

670 Regarding the proposed water management plan for the ice sluicing target, based on the proposed
671 results, it is needed to take into account the hydrological and meteorological conditions that are
672 simulated in the study. Furthermore, since results show a potential ice stoppage based on the shape
673 of the islands, a practical solution would be to redesigning the islands into more rounded shapes.

674 This newly presented method embrace a wide type of inland water areas including lowland rivers
675 and reservoirs. This approach does not perquisite the ice stoppage criteria like the location and
676 velocity threshold. The model is based on the 2 novel methods of comparing the original and final ice
677 thickness, and the ice velocity to the water velocity. Referring to the limitation of the approach,
678 major required data would be mentioned; for instance, hydrodynamic, bathymetric, and ice
679 condition data.

680 **Acknowledgments**

681 The bathymetry data used in the Odra River study were provided by Sweco Consulting and were part
682 of the Odra-Vistula Flood Management Project – 8524 PI, Sub-component 1A: Flood protection of
683 areas in Zachodniopomorskie Voivodeship. The Vistula River study was supported by the National
684 Water Management Authority ‘Wody Polskie’ Project no KZGW/KS/306/2019. The author wishes to
685 show the appreciation to the anonymous reviewers for their careful reading of the manuscript and
686 their many insightful comments and suggestions.

687 **Literature**

- 688 Ashton, G.D., 1986. River and lake ice engineering. Water Resources Publication, Littleton Co, USA.
689 Ashton, G.D., 1978. River ice. *Annu. Rev. Fluid Mech.* 10, 369–392.
690 Babiński, Z., 1982. Influence of the water dam in Włocławek on fluvial processes of the Vistula River.
691 Polish Academy of Sciences, Institute of Geography and Spatial Organization.
692 Beltaos, S., 2018. The 2014 ice-jam flood of the Peace-Athabasca Delta: Insights from numerical
693 modelling. *Cold Reg. Sci. Technol.* 155, 367–380.
694 Beltaos, S., 2003. Numerical modelling of ice-jam flooding on the Peace–Athabasca delta. *Hydrol.*
695 *Process.* 17, 3685–3702.
696 Beltaos, S., 1995. River Ice Jams. Water Resources Publication.
697 Beltaos, S., 1983. River ice jams: theory, case studies, and applications. *J. Hydraul. Eng.* 109, 1338–
698 1359.
699 Beltaos, S., Burrell, B.C., 2015. Hydroclimatic aspects of ice jam flooding near Perth-Andover, New
700 Brunswick. *Can. J. Civ. Eng.* 42, 686–695.
701 Boucher, É., Bégin, Y., Arseneault, D., 2009. Impacts of recurring ice jams on channel geometry and
702 geomorphology in a small high-boreal watershed. *Geomorphology* 108, 273–281.
703 Boucher, E., Bégin, Y., Arseneault, D., Ouarda, T.B., 2012. Long-term and large-scale river-ice
704 processes in cold-region watersheds. *Gravel-Bed Rivers Process. Tools Environ.* 546–554.
705 Brunner, G.W., 2002. Hec-ras (river analysis system), in: North American Water and Environment
706 Congress & Destructive Water. ASCE, pp. 3782–3787.

- 707 Carson, R., Beltaos, S., Groeneveld, J., Healy, D., She, Y., Malenchak, J., Morris, M., Saucet, J.-P.,
708 Kolarski, T., Shen, H.T., 2011. Comparative testing of numerical models of river ice jams. *Can.*
709 *J. Civ. Eng.* 38, 669–678. <https://doi.org/10.1139/l11-036>
- 710 Das, A., Lindenschmidt, K.-E., 2020. Evaluation of the sensitivity of hydraulic model parameters,
711 boundary conditions and digital elevation models on ice-jam flood delineation. *Cold Reg. Sci.*
712 *Technol.* 103218.
- 713 Flato, G., Gerard, R., 1986. Calculation of ice jam thickness profiles, in: *Proc., 4th Workshop on Hydr.*
714 *of River Ice.* pp. 1–25.
- 715 Gosztowtt, J., 2018. Spatio-temporal changes of Vistula riverbed below the Włocławek hydropower
716 plant (MSc Thesis). University of Salzburg, Salzburg.
- 717 Grześ, M., 1991. Ice jams and floods on the lower Vistula river: mechanism and processes. Polish
718 Academy of Sciences Institute of Geography and Spatial Organization, Warsaw.
- 719 Hicks, F.E., Steffler, P.M., Gerard, R., 1992. Finite element modeling of surge propagation and an
720 application to the Hay River, N.W.T. *Can. J. Civ. Eng.* 19, 454–462.
721 <https://doi.org/10.1139/l92-055>
- 722 Ji, S., Shen, H.T., Wang, Z., Shen, H.H., Yue, Q., 2005. A viscoelastic-plastic constitutive model with
723 Mohr-Coulomb yielding criterion for sea ice dynamics. *ACTA Oceanol. Sin.-Engl. Ed.-* 24, 54.
- 724 Kandamby, A., Jayasundara, N., Shen, H.T., Deyhle, C., 2010. A numerical river ice model for Elbe
725 River, in: 20th IAHR International Symposium on Ice. Lahti, Finland. Lahti, Finland.
- 726 Knack, I.M., Shen, H.T., 2018. A numerical model for sediment transport and bed change with river
727 ice. *J. Hydraul. Res.* 56, 844–856.
- 728 Knack, I.M., Shen, H.T., 2017. Numerical modeling of ice transport in channels with river restoration
729 structures. *Can. J. Civ. Eng.* 44, 813–819. <https://doi.org/10.1139/cjce-2017-0081>
- 730 Knack, I.M., Shen, H.T., 2016. A numerical model study on Saint John River ice breakup. *Can. J. Civ.*
731 *Eng.* 45, 817–826.
- 732 Kolarski, T., 2018. Mathematical modeling of ice dynamics as a decision support tool in river
733 engineering. *Water* 10, 1241.
- 734 Kolarski, T., 2016. Modeling of Ice Passage Through Reservoirs System on the Vistula River, in:
735 Rowiński, P., Marion, A. (Eds.), *Hydrodynamic and Mass Transport at Freshwater Aquatic*
736 *Interfaces: 34th International School of Hydraulics, GeoPlanet: Earth and Planetary Sciences.*
737 Springer International Publishing, Cham, pp. 35–47. [https://doi.org/10.1007/978-3-319-](https://doi.org/10.1007/978-3-319-27750-9_4)
738 [27750-9_4](https://doi.org/10.1007/978-3-319-27750-9_4)
- 739 Kolarski, T., Huang, F., Shen, H.T., 2016. Development of Ice Jam Toe Configurations. Presented at the
740 23 rd IAHR International Symposium on Ice, Ann Arbor, Michigan USA.
- 741 Kolarski, T., Shen, H.T., 2015. Possible effects of the 1984 St. Clair River ice jam on bed changes. *Can.*
742 *J. Civ. Eng.* 42, 696–703.
- 743 Kovachis, N., Burrell, B.C., Huokuna, M., Beltaos, S., Turcotte, B., Jasek, M., 2017. Ice-jam flood
744 delineation: Challenges and research needs. *Can. Water Resour. Journal/Revue Can. Ressour.*
745 *Hydr.* 42, 258–268.
- 746 Kreft, A., Parzonka, W., 2007. Issues related to the modernization of river regulation structures on
747 the border section of the Lower Odra river. *Infrastruct. Ecol. Rural Areas* 123–134.
- 748 Lal, A.W., Shen, H.T., 1991. Mathematical model for river ice processes. *J. Hydraul. Eng.* 117, 851–
749 867.
- 750 Lindenschmidt, K.-E., Carstensen, D., Fröhlich, W., Hentschel, B., Iwicki, S., Kögel, M., Kubicki, M.,
751 Kundzewicz, Z.W., Lauschke, C., Łazarów, A., 2019. Development of an Ice Jam Flood
752 Forecasting System for the Lower Oder River—Requirements for Real-Time Predictions of
753 Water, Ice and Sediment Transport. *Water* 11, 95.
- 754 Lindenschmidt, K.E., Rokaya, P., 2019. A Stochastic Hydraulic Modelling Approach to Determining the
755 Probable Maximum Staging of Ice-Jam Floods. *J. Environ. Inform.* 34.
- 756 Lindenschmidt, K.-E., Sydor, M., Carson, R.W., 2012. Modelling ice cover formation of a lake–river
757 system with exceptionally high flows (Lake St. Martin and Dauphin River, Manitoba). *Cold*
758 *Reg. Sci. Technol.* 82, 36–48.

- 759 Liu, L., Shen, H.T., 2005. Numerical modeling of 2003 Grasse River ice jam and scenario analysis.
760 Presented at the Proc., 13th Workshop of the Hydraulics of Ice Covered Rivers, Hanover, NH,
761 USA.
- 762 Marszelewski, W., Pawłowski, B., 2019. Long-Term Changes in the Course of Ice Phenomena on the
763 Oder River along the Polish–German Border. *Water Resour. Manag.* 33, 5107–5120.
764 <https://doi.org/10.1007/s11269-019-02417-2>
- 765 Mudelsee, M., Börngen, M., Tetzlaff, G., Grünewald, U., 2004. Extreme floods in central Europe over
766 the past 500 years: Role of cyclone pathway “Zugstrasse Vb.” *J. Geophys. Res. Atmospheres*
767 109.
- 768 Pariset, E., Hauser, R., 1961. FORMATION AND EVOLUTION OF ICE COVERS ON RIVERS. *Trans. Eng.*
769 *Inst. Can.* 5, 41–49.
- 770 Pariset, E., Hausser, R., Gagnon, A., 1966. Formation of Ice Covers and Ice Jams in Rivers. *J. Hydraul.*
771 *Div.* 92, 1–24.
- 772 Pawłowski, B., 2019. Ice Jams: Causes and Effects, in: *Encyclopedia of Water*. American Cancer
773 Society, pp. 1–9. <https://doi.org/10.1002/9781119300762.wsts0035>
- 774 Pawłowski, B., 2015. Determinants of change in the duration of ice phenomena on the Vistula River
775 in Toruń. *J. Hydrol. Hydromech.* 63. <https://doi.org/10.1515/johh-2015-0017>
- 776 Prowse, T.D., 1990. Heat and mass balance of an ablating ice jam. *Can. J. Civ. Eng.* 17, 629–635.
- 777 Rădoane, M., Ciaglic, V., Rădoane, N., 2010. Hydropower impact on the ice jam formation on the
778 upper Bistrita River, Romania. *Cold Reg. Sci. Technol.* 60, 193–204.
779 <https://doi.org/10.1016/j.coldregions.2009.10.006>
- 780 RWMA, 2010. Icebreaking operation 2009/2010 report. Regional Water Management Authority in
781 Szczecin, Szczecin.
- 782 RWMA, W., 2009. Instruction of icebreaking and ice sluicing thorough Włocławek Dam (No. XI).
783 Regional Water Management Authority, Warszawa.
- 784 Schneck, C.C., Ghobrial, T.R., Loewen, M.R., 2019. Laboratory study of the properties of frazil ice
785 particles and flocs in water of different salinities. *Cryosphere* 13.
- 786 Shen, H.T., 2016. River Ice Processes, in: Wang, L.K., Yang, C.T., Wang, M.-H.S. (Eds.), *Advances in*
787 *Water Resources Management*. Springer International Publishing, Cham, pp. 483–530.
788 https://doi.org/10.1007/978-3-319-22924-9_9
- 789 Shen, H.T., 2010. Mathematical modeling of river ice processes. *Cold Reg. Sci. Technol.* 62, 3–13.
790 <https://doi.org/10.1016/j.coldregions.2010.02.007>
- 791 Shen, H.T., Gao, L., Kolarski, T., Liu, L., 2008. Dynamics of Ice Jam Formation and Release. *J. Coast.*
792 *Res.* 52, 25–32. <https://doi.org/10.2112/1551-5036-52.sp1.25>
- 793 Shen, H.T., Jayasundara, N.C., Tuthill, A.M., Mihm, J.E., 2005. Frequency and Severity of Past Ice Jams
794 on the Grass River. Presented at the 13 th Workshop on the Hydraulics of Ice Covered Rivers,
795 Hanover, NH, USA, p. 8.
- 796 Shen, H.T., Liu, L., 2003. Shokotsu River ice jam formation. *Cold Reg. Sci. Technol.* 37, 35–49.
- 797 Shen, H.T., Shen, H., Tsai, S.-M., 1990. Dynamic transport of river ice. *J. Hydraul. Res.* 28, 659–671.
- 798 Shen, H.T., Su, J., Liu, L., 2000. SPH Simulation of River Ice Dynamics. *J. Comput. Phys.* 165, 752–770.
799 <https://doi.org/10.1006/jcph.2000.6639>
- 800 Staśko, S., Buczyński, S., 2018. Drought and its effects on spring discharge regimes in Poland and
801 Germany during the 2015 drought. *Hydrol. Sci. J.* 63, 741–751.
802 <https://doi.org/10.1080/02626667.2018.1446215>
- 803 Su, J., Shen, H.T., Crissman, R.D., 1997. Numerical study on ice transport in vicinity of Niagara River
804 hydropower intakes. *J. Cold Reg. Eng.* 11, 255–270.
- 805 Svensson, U., Billfalk, L., Hammar, L., 1989. A mathematical model of border-ice formation in rivers.
806 *Cold Reg. Sci. Technol.* 16, 179–189.
- 807 Szydłowski, M., Gąsiorowski, D., Szymkiewicz, R., Zima, P., Hakiel, J., 2015. Hydropower potential of
808 the lower Vistula. *Acta Energ.* 1, 18–25.

- 809 Szydłowski, M., Kolerski, T., 2018. Numerical Modeling of Water and Ice Dynamics for Analysis of
810 Flow Around the Kiezmark Bridge Piers, in: *Free Surface Flows and Transport Processes*.
811 Springer, pp. 465–476.
- 812 Szymkiewicz, R., 2017. Dolna Wisła-rzeka niewykorzystanych możliwości. Wydawnictwo Politechniki
813 Gdańskiej.
- 814 Thériault, I., Saucet, J.-P., Taha, W., 2010. Validation of the Mike-Ice model simulating river flows in
815 presence of ice and forecast of changes to the ice regime of the Romaine river due to
816 hydroelectric project, in: *Proceedings of the 20th IAHR International Symposium on Ice*,
817 Lahti, Finland.
- 818 Timalsina, N.P., Charmasson, J., Alfredsen, K.T., 2013. Simulation of the ice regime in a Norwegian
819 regulated river. *Cold Reg. Sci. Technol.* 94, 61–73.
- 820 Timoney, K., Peterson, G., Fargey, P., Peterson, M., McCanny, S., Wein, R., 1997. Spring ice-jam
821 flooding of the Peace-Athabasca Delta: Evidence of a climatic oscillation. *Clim. Change* 35,
822 463–483.
- 823 Tuthill, A., Ashton, G., Hendershot, P., Quadrini, J., 2008. Grasse River Ice Control Structure, Physical
824 Model Study. Presented at the 19th IAHR International Symposium on Ice, Vancouver, BC,
825 Canada, p. 11.
- 826 Uzuner, M.S., Kennedy, J.F., 1976. Theoretical model of river ice jams. *J. Hydraul. Div.* 102.
- 827 Uzuner, M.S., Kennedy, J.F., 1974. Hydraulics and mechanics of river ice jams. IOWA INST OF
828 HYDRAULIC RESEARCH IOWA CITY.
- 829 Wang, J., Shi, F., Chen, P., Wu, P., Sui, J., 2015. Impact of bridge pier on the stability of ice jam. *J.*
830 *Hydrodyn.* 27, 865–871. [https://doi.org/10.1016/S1001-6058\(15\)60549-2](https://doi.org/10.1016/S1001-6058(15)60549-2)
- 831 White, K.D., 1999. Hydraulic and physical properties affecting ice jams.
- 832 Wolfe, B.B., Hall, R.I., Wiklund, J.A., Kay, M.L., 2020. Past variation in Lower Peace River ice-jam flood
833 frequency. *Environ. Rev.* 1–9.
- 834 Wolski, K., Tymiński, T., Głuchowska, B., 2017. Analysis of ice phenomena hazard on the middle Odra
835 river. *Ann. Wars. Univ. Life Sci. – SGGW Land Reclam.* 49. [https://doi.org/10.1515/ssgw-](https://doi.org/10.1515/ssgw-2017-0024)
836 [2017-0024](https://doi.org/10.1515/ssgw-2017-0024)
- 837 Wu, J., 1973. Prediction of near-surface drift currents from wind velocity. *J. Hydraul. Div.* 99, 1291–
838 1302.

839